

Bayesian Invariance Modeling of Multi-Environment Data

Luhuan Wu[†], Mingzhang Yin[#], Yixin Wang^{*},

John P. Cunningham[†], David M. Blei^{†,‡,*}

Abstract

Invariant prediction [Peters et al., 2016] analyzes feature/outcome data from multiple environments to identify *invariant features*—those with a stable predictive relationship to the outcome. Such features support generalization to new environments and help reveal causal mechanisms. Previous methods have primarily tackled this problem through hypothesis testing or regularized optimization. Here we develop *Bayesian Invariant Prediction (BIP)*, a probabilistic model for invariant prediction. BIP encodes the indices of invariant features as a latent variable and recover them by posterior inference. Under the assumptions of Peters et al. [2016], the BIP posterior targets the true invariant features. We prove that the posterior is consistent and that greater environment heterogeneity leads to faster posterior contraction. To handle many features, we design an efficient variational approximation called *VI-BIP*. In simulations and real data, we find that BIP and VI-BIP are more accurate and scalable than existing methods for invariant prediction.

Keywords: Bayesian Modeling; Feature Selection; Invariant Prediction; Variational Inference.

^{*†}Department of Statistics, Columbia University. [‡]Department of Computer Science, Columbia University. [#]Warrington College of Business, University of Florida. ^{*}Department of Statistics, University of Michigan.

Address for correspondence: Luhuan Wu, Department of Statistics, Columbia University, 1255 Amsterdam Avenue, New York, NY, 10027, USA. Email: lw2827@columbia.edu

1 Introduction

An important goal of statistics is to identify features that have stable effects across varying settings and conditions. This ability is important for building robust prediction models that generalize well to novel situations, and for uncovering causal mechanisms to inform effective interventions.

To this end, [Peters et al. \[2016\]](#) introduced the problem of *invariant prediction*. In this problem, we are given feature/outcome data from multiple *environments*, each involving a different data-generating distribution. Our goal is to find the set of features that are *invariant* to the environment, i.e., those that govern the outcome in the same way across all environments. To solve the problem, existing algorithms either search over invariant sets and use hypothesis testing [[Peters et al., 2016](#)], or frame the problem as a regularized optimization that encourages an invariant solution [[Fan et al., 2023](#)].

In this paper, we introduce *Bayesian Invariant Prediction (BIP)*. We design a probabilistic model of multi-environment data, where the invariant set is encoded as a latent variable, and we infer the invariant set through Bayesian posterior inference. The BIP posterior targets the true invariant solution, and it provides a model-based quantification of uncertainty about the invariant set. We investigate BIP theoretically and empirically.

How does BIP work? At its core, [Peters et al. \[2016\]](#) makes two assumptions about the data-generating process for invariant prediction:

1. The p features x^1, \dots, x^p follow different distributions across environments.
2. The outcome y depends on a subset of x in the same way across environments; this subset is the *invariant set*.

BIP explicitly bakes these data-generating assumptions into a joint distribution of the invariant feature set and multi-environment data. We model the outcome, conditional on the invariant features, to be independent of the environment, and we explicitly model the per-environment distributions of the features. (We note that [Peters et al. \[2016\]](#) also assumes a linear data-generating process. Here we do not make linear assumptions.)

Crucially, the invariant feature set is treated as a latent variable.

Originally, [Peters et al. \[2016\]](#) motivated these assumptions through a causal problem. Each environment arises by an unknown intervention on the features x ; the outcome y is directly caused by a subset of those features; and the goal is to analyze the multi-environment data to determine the direct causes of y . Here we solve the same problem but state the invariance assumption directly without appealing to causality. While these assumptions often arise from a causal problem, invariance has wider applications including predictive robustness [[Bühlmann, 2020](#)], domain adaptation [[Rojas-Carulla et al., 2018](#)], and out-of-distribution generalization [[Arjovsky et al., 2019](#)].

In detail, BIP models data from E environments, $\mathcal{D} = \{\{x_{ei}, y_{ei}\}_{i=1}^{n_e}\}_{e=1}^E$, where x_{ei} is a vector of p features and y_{ei} is an outcome. We encode the latent invariant feature set through a feature selection vector $z \in \{0, 1\}^p$, where each entry $z^{(i)}$ indicates the inclusion of the i -th feature. Let x^z denote the subvector of features where $z^{(i)} = 1$ and x^{-z} the subvector where $z^{(i)} = 0$. With this notation, the BIP model factorizes as follows

$$p(z, \mathcal{D}) = p(z) \prod_{e=1}^E \prod_{i=1}^{n_e} p_e(x_{ei}^z) g(y_{ei} | x_{ei}^z) p_e(x_{ei}^{-z} | y_{ei}, x_{ei}^z). \quad (1)$$

Notice where the distribution depends on the environment p_e and where it is invariant g . As a generative process, the model says that each environment first produces the invariant features from a per-environment distribution; then produces the outcome from an invariant conditional distribution; and finally produces the non-invariant features from a per-environment distribution, conditional on the invariant features and the outcome.

Given multi-environment data, we can use this model to calculate the posterior distribution of the invariant set $p(z | \mathcal{D})$. We prove that this posterior distribution is consistent under the data generating assumptions of [Peters et al. \[2016\]](#), targeting the true invariant features. We also analyze the posterior contraction rate with respect to the per-environment sample size and the number of environments, and characterize its dependence on the prior of z and the heterogeneity of the environments.

Similar to the hypothesis testing method in [Peters et al. \[2016\]](#), exact posterior in-

ference for BIP requires searching over 2^p possible sets of invariant features. When p is large, exact inference is computationally prohibitive. To address this challenge, we develop *VI-BIP* a variational inference (VI) algorithm [Jordan et al., 1999, Blei et al., 2017] to approximate the posterior. VI-BIP finds a p -vector of approximate posterior probabilities that each feature is in the invariant set. Algorithmically, it optimizes a variational objective over the discrete feature selector. In this way, it resembles some of the optimization-based approaches to invariant prediction that optimize continuous regression parameters with regularization [Arjovsky et al., 2019, Yin et al., 2024]. Compared to exact inference, VI-BIP does not require an exhaustive exponential search.

We study BIP and VI-BIP on both simulated and real data, comparing performance to existing approaches [Peters et al., 2016, Rothenhäusler et al., 2019, Fan et al., 2023]. The simulation study verifies our theoretical findings and demonstrates improved accuracy and scalability of our methods compared to existing works. In particular, VI-BIP performs competitively with exact inference in low-dimensional settings, while remaining scalable to high-dimensional cases. In a real-world study, we examine gene perturbation data that includes $p = 6,179$ features [Kemmeren et al., 2014]. VI-BIP outperforms existing methods by identifying more true effects based on the inferred invariant features. As a comparison, existing methods are sensitive to the required feature screening step, which usually results in either overly conservative predictions or false predictions.

We summarize our contributions as follows:

1. We design *Bayesian Invariant Prediction (BIP)* for multi-environment data. It encodes the invariance assumption and enables posterior inference of the invariant features.
2. We establish theoretical guarantees for BIP, including posterior consistency and contraction rates.
3. We develop *VI-BIP*, a scalable variational inference algorithm for high-dimensional settings. It overcomes the exponential complexity of exact BIP inference.

4. On simulated and real-world data, we demonstrate that BIP outperforms existing approaches in terms of inference accuracy and scalability.

The paper is organized as follows. In § 2 we state the main invariance assumption and introduce BIP, including the model structure, exact inference procedure, and the scalable variational approximation. In § 3, we present theoretical results on posterior consistency and contraction rates. In § 4, we validate BIP on simulations. In § 5, we use BIP to study real data. In § 6, we summarize BIP and discuss limitations and future work.

1.1 Related works

Invariance closely relates to the independent causal mechanism in causal inference literature [Peters et al., 2017, Schölkopf et al., 2021], which states that the causal mechanism $p(y|x)$ and the cause distribution $p(x)$ are independent under the causal structure $x \rightarrow y$. This property implies the possibility of intervening on $p(x)$ while keeping $p(y|x)$ invariant. Invariance was also studied in econometrics under the terms autonomy and modularity [Frisch et al., 1948, Hoover, 2008], and later appeared in computer science as stable and autonomous parent-child relationships in causal graphs [Pearl, 2009, p. 22]. For a historical overview of invariance, see Peters et al. [2017, Chapter 2.2] and Bühlmann [2020].

Peters et al. [2016] is the seminal work that formalized the concept of invariant prediction for machine learning problems, as well as connecting it to causal inference. It assumes that the distribution of the outcome given a subset of features remains the same across environments, and under certain conditions, these features are the direct causes of the outcome. It develops a hypothesis testing approach for identifying such features in linear models, which requires an exhaustive search over exponentially many candidates.

Since Peters et al. [2016], invariant prediction has become an active area of research. Heinze-Deml et al. [2018] extends this framework to non-linear settings. Rothenhäusler et al. [2019] proposes an invariance notion based on feature-residual inner products in linear models, inking it to causal inference under additive interventions. Fan et al. [2023] incorporates residual-based invariance as a regularization term in linear regression. Wang

et al. [2024] establishes a theoretical connection between invariant prediction models and causal outcome models, leading to a computationally efficient algorithm for causal discovery. Gu et al. [2025] shows that solving for exact invariance is NP-hard and introduces an objective that interpolates between exact invariance and predictive performance.

This paper offers a new perspective on invariant prediction, by introducing a Bayesian approach. In this sense, our goals are most close aligned to Peters et al. [2016] and Fan et al. [2023]. As we will see below, our probabilistic perspective on this problem opens the door to both new algorithms and new theoretical understanding.

2 Bayesian Invariant Prediction

2.1 Multi-environment data and the invariance assumption

Consider a dataset of feature-outcome pairs that are organized into *multiple environments*, $\mathcal{D} := \{\{x_{ei}, y_{ei}\}_{i=1}^{n_e}\}_{e=1}^E$. In each pair, x is a p -dimensional vector and y is a general outcome. Each environment e indexes a distinct data distribution $p_e(x, y)$, and x_{ei}, y_{ei} were drawn IID from this distribution.

Our main assumption is that some of the features are *invariant*—the conditional distribution of the outcome given these features remains unchanged across all environments [Peters et al., 2016]. We formally state this assumption as follows:

Assumption 1 (Invariance). *Consider a collection of environments \mathcal{E} . Then $\exists z^* \in \{0, 1\}^p$ such that $p_e(y \mid x^{z^*})$ is invariant with respect to $e \in \mathcal{E}$.*

We call z^* the (*true*) *invariant feature selector* and x^{z^*} the (*true*) *invariant features*. As a consequence of Assumption 1 and the chain rule, each environment’s joint distribution factorizes,

$$p_e(x, y) = p_e(x^{z^*})p_*(y \mid x^{z^*})p_e(x^{-z^*} \mid x^{z^*}, y). \quad (2)$$

The invariant conditional $p_*(y \mid x^{z^*}) \equiv p_e(y \mid x^{z^*})$ for all environments $e \in \mathcal{E}$.

The problem is that we do not observe the invariant feature selector z^* . Our goal is to infer z^* from the observed multi-environment data.

2.2 A Bayesian model of invariant prediction

We propose Bayesian Invariant Prediction (BIP) to infer the true invariant features z^* . Our model places a prior distribution $p(z)$ over feature selectors $z \in \{0, 1\}^p$ and defines a likelihood based on the invariance assumption.

For now, we assume the local joint distributions $\{p_e(x, y)\}_{e=1}^E$ are known. Consequently, for any candidate invariant feature selector z , we can calculate the *local marginal* $p_e(x^z)$, *local conditionals* $p_e(y|x^z)$, and *local feature conditionals* $p_e(x^{-z} | x^z, y)$, all derived from the local joint $p_e(x, y)$. In practice, we can estimate these distributions with a sufficiently large dataset.

To build our likelihood, we also define a *pooled conditional distribution* of the outcome given candidate features x^z , derived from the collection of local distributions.

Definition 1 (Pooled conditional). *Given a feature selector z and a collection of local distributions $\{p_e(x, y)\}_{e \in \mathcal{E}}$, define the pooled conditional as:*

$$g(y | x^z) := \frac{\sum_{e \in \mathcal{E}} \int p_e(x, y) dx^{-z}}{\sum_{e \in \mathcal{E}} p_e(x^z)}.$$

The pooled conditional characterizes the distribution of outcome y given candidate features x^z , based on distributions pooled across environments. In BIP, the pooled conditional will serve as the invariant distribution of the outcome. Its key property is that it matches the local conditional distributions $p_e(y | x^z)$ simultaneously across all environments if and only if $z = z^*$. Therefore it will help the posterior center on the true invariant feature selector. We state this idea formally as follows.

Proposition 1 (Identifiability of invariant features). *Under Assumption 1, the equality*

$$g(y | x^z) = p_e(y | x^z), \quad \forall e \in \mathcal{E},$$

holds if and only if $z = z^*$.

Proof If $z = z^*$, then by definition of invariance (Assumption 1), $p_e(y \mid x^{z^*})$ is identical across environments. Substituting the true factorization from Eq. 2 into the pooled definition shows equality. Conversely, if $g(y \mid x^z)$ matches each environment’s local conditional distribution $p_e(y \mid x^z)$ simultaneously, then these local distributions must themselves be identical across environments. Thus z must satisfy Assumption 1, making $z = z^*$. ■

With the pooled conditional in hand, we now define the BIP model for invariant feature selection:

- Draw invariant feature selector $z \sim p(z)$.
- For $e = 1, \dots, E \in \mathcal{E}$, and each observation $i = 1, \dots, n_e$:
 1. Draw invariant features $x_{ei}^z \sim p_e(x_{ei}^z)$.
 2. Draw outcome $y_{ei} \mid x_{ei}^z \sim g(y_{ei} \mid x_{ei}^z)$.
 3. Draw remaining features $x_{ei}^{-z} \mid x_{ei}^z, y_{ei} \sim p_e(x_{ei}^{-z} \mid x_{ei}^z, y_{ei})$.

The BIP model encodes invariance. Step 2 explicitly uses the pooled conditional, thereby enforcing a single conditional distribution for $y \mid x^z$ across environments. The joint distribution of latent and observed variables was introduced earlier in Eq. 1.

Under Assumption 1, the BIP’s posterior will concentrate around the true invariant selector z^* . For any candidate $z \neq z^*$, the pooled conditional $g(y \mid x^z)$ cannot match all the true local distributions $p_e(y \mid x^z)$, resulting in a lower data likelihood and posterior probability. But when $z = z^*$, the pooled conditional matches all local distributions exactly, leading to maximal likelihood and a posterior centered around the truth.

To see this observation more concretely, we write the posterior distribution explicitly as a product of prior and likelihood ratios – each between the pooled conditional and a local conditional. This expression is a key property of our model.

Proposition 2 (Posterior expression). *Under the BIP model in Eq. 1, the posterior distribution simplifies to:*

$$p(z \mid \mathcal{D}) \propto p(z) \prod_{e=1}^E \prod_{i=1}^{n_e} \frac{g(y_{ei} \mid x_{ei}^z)}{p_e(y_{ei} \mid x_{ei}^z)}. \quad (3)$$

Proof Start from the joint distribution under the model:

$$p(z, \mathcal{D}) = p(z) \prod_{e=1}^E \prod_{i=1}^{n_e} p_e(x_{ei}^z) g(y_{ei} \mid x_{ei}^z) p_e(x_{ei}^{-z} \mid x_{ei}^z, y_{ei}).$$

Multiplying a constant of 1 in the form of $p_e(y_{ei} \mid x_{ei}^z)/p_e(y_{ei} \mid x_{ei}^z)$, we obtain

$$p(z, \mathcal{D}) = p(z) \prod_{e=1}^E \prod_{i=1}^{n_e} p_e(x_{ei}^z) g(y_{ei} \mid x_{ei}^z) p_e(x_{ei}^{-z} \mid x_{ei}^z, y_{ei}) \frac{p_e(y_{ei} \mid x_{ei}^z)}{p_e(y_{ei} \mid x_{ei}^z)}.$$

Note that $p_e(x_{ei}^z) p_e(y_{ei} \mid x_{ei}^z) p_e(x_{ei}^{-z} \mid x_{ei}^z, y_{ei}) = p_e(x_{ei}, y_{ei})$. So,

$$p(z, \mathcal{D}) = p(z) \prod_{e=1}^E \prod_{i=1}^{n_e} p_e(x_{ei}, y_{ei}) \frac{g(y_{ei} \mid x_{ei}^z)}{p_e(y_{ei} \mid x_{ei}^z)}.$$

The local joint distribution $p_e(x_{ei}, y_{ei})$ is constant with respect to z . Therefore we obtain the simplified posterior of Eq. 3. ■

This expression for the posterior highlights the role of the ratio between the pooled conditional and the local conditionals, and shows that the posterior centers on the true invariant feature selector. For choices of $z \neq z^*$, the pooled conditional $g(y \mid x^z)$ differs from the true local distributions $p_e(y \mid x^z)$, decreasing the likelihood ratio. However, at $z = z^*$, Proposition 1 guarantees equality between the pooled and local conditionals, maximizing this ratio. Thus the posterior concentrates around the true z^* . We formalize this intuition through posterior consistency and contraction results in § 3.

Note that the likelihood ratio between pooled and local conditionals precisely targets the invariance criteria in the frequentist framework of [Peters et al. \[2016\]](#). In that framework, a likelihood ratio of one corresponds to the null hypothesis being satisfied,

indicating invariance. Here, the likelihood ratio naturally arises from our distributional assumptions and a probabilistic modeling perspective.

2.3 Exact posterior inference for BIP

We now turn to the problem of calculating the posterior. In practice, we do not have access to the true data distributions $p_e(x, y)$ and must estimate them. In principle we could estimate these full joint distributions from data. But note that the simplified posterior expression in Eq. 3 depends only on the local conditionals $p_e(y \mid x^z)$ and pooled conditional $g(y \mid x^z)$ for each feature selector z . So, we directly model these relevant conditionals. Specifically, let $\mathcal{P}_{y|x^z}$ be a conditional model class indexed by z . We estimate local and pooled conditionals, respectively, via maximum likelihood:

$$\hat{p}_e(y \mid x^z) := \arg \max_{\tilde{p}(y|x^z) \in \mathcal{P}_{y|x^z}} \sum_{i=1}^{n_e} \log \tilde{p}(y_{ei} \mid x_{ei}^z), \quad \forall e, z \quad (4)$$

$$\hat{g}(y \mid x^z) := \arg \max_{\tilde{p}(y|x^z) \in \mathcal{P}_{y|x^z}} \sum_{e=1}^E \sum_{i=1}^{n_e} \log \tilde{p}(y_{ei} \mid x_{ei}^z), \quad \forall z. \quad (5)$$

We then compute the posterior distribution explicitly by iterating over all candidate feature selectors z according to Eq. 3:

$$\hat{p}(z \mid \mathcal{D}) \propto p(z) \prod_{e \in \mathcal{E}} \prod_{i=1}^{n_e} \frac{\hat{g}(y_{ei} \mid x_{ei}^z)}{\hat{p}_e(y_{ei} \mid x_{ei}^z)}. \quad (6)$$

The exact posterior inference procedure is summarized in Algorithm 1. The algorithm explicitly enumerates all candidate feature selectors, estimates the local and pooled conditionals, and calculates the posterior probabilities accordingly.

This procedure can be expensive. When the prior $p(z)$ has full support on $\{0, 1\}^p$, the complexity of PI-exact is $O(2^p \cdot c(\mathcal{D}, p))$, where $c(\mathcal{D}, p)$ is the cost of estimating and evaluating the conditional models in Eq. 4 and Eq. 5 from data with up to p features. With prior information restricting the support of $p(z)$ to subsets of size at most p_{\max} ,

Algorithm 1: BIP: exact posterior inference for invariant features

Input: Dataset $\mathcal{D} = \{(x_{ei}, y_{ei})\}$

Output: Posterior distribution $\hat{p}(z \mid \mathcal{D})$

- 1 **for** z in support of $p(z)$ **do**
 - 2 Estimate local conditionals $\{\hat{p}_e(y \mid x^z)\}_{e=1}^E$ and pooled conditional $\hat{g}(y \mid x^z)$ via Eq. 4 and Eq. 5;
 - 3 Compute the likelihood ratio: $\hat{\Lambda}(z) \leftarrow \prod_{e=1}^E \prod_{i=1}^{n_e} \frac{\hat{g}(y_{ei} \mid x_{ei}^z)}{\hat{p}_e(y_{ei} \mid x_{ei}^z)}$.
 - 4 Compute the posterior: $\hat{p}(z \mid \mathcal{D}) \propto p(z) \hat{\Lambda}(z)$.
-

Algorithm 2: VI-BIP: variational inference for invariant features

Input: Dataset \mathcal{D} , iterations T , number of gradient samples M , learning rate scheduler $r(\cdot)$

Output: Variational posterior $q_{\phi_T}(z)$

- 1 Initialize variational parameter ϕ_0
 - 2 **for** $t = 1$ **to** T **do**
 - 3 Compute M unbiased gradient estimates of the ELBO using U2G (Algorithm 3, see the supplementary materials): $\hat{h}_m \approx \nabla_{\phi} \mathcal{L}(\mathcal{D}, \phi_{t-1})$ for $m = 1, \dots, M$
 - 4 Update variational parameters: $\phi_t \leftarrow \phi_{t-1} + r(t) \cdot \frac{1}{M} \sum_{m=1}^M \hat{h}_m$
-

the complexity reduces to $O(p^{p_{\max}} \cdot c(\mathcal{D}, p_{\max}))$. However, this complexity may still be prohibitive for large p . In the next section, we introduce a scalable variational inference method suitable for high-dimensional settings.

2.4 Variational inference for BIP

Exact posterior inference (§ 2.3) enumerates all possible invariant selectors, which is infeasible for large feature sets. Here we turn to variational inference [VI, Blei et al., 2017] to develop VI-BIP, an approximate inference algorithm to estimate the posterior.

VI approximates the posterior with a simpler distribution. We posit a mean-field family of approximate posterior distributions of z :

$$q_{\phi}(z) := \prod_{j=1}^p \text{Bernoulli}(z^{(j)} \mid \text{sigmoid}(\phi^{(j)})),$$

where $\text{sigmoid}(\cdot) := \frac{\exp(\cdot)}{1 + \exp(\cdot)}$, and $\phi \in \mathbb{R}^p$ are the variational parameters. We then fit these

parameters by maximizing the evidence lower bound (ELBO),

$$\begin{aligned}\mathcal{L}(\mathcal{D}, \phi) &= \mathbb{E}_{q_\phi(z)} [\log p(z, \mathcal{D}) - \log q_\phi(z)] \\ &= \mathbb{E}_{q_\phi(z)} \left[\log p(z) + \sum_{e=1}^E \sum_{i=1}^{n_e} \log \frac{g(y_{ei} | x_{ei}^z)}{p_e(y_{ei} | x_{ei}^z)} - \log q_\phi(z) \right] + C,\end{aligned}\tag{7}$$

where $C = \sum_{e=1}^E \sum_{i=1}^{n_e} \log p(x_{ei}, y_{ei})$ is a constant with respect to ϕ . The optimal variational parameters minimize the KL divergence to the exact posterior.

In detail, we first estimate $\hat{g}(y | x^z)$ and $\hat{p}_e(y | x^z)$ from data, and then optimize Eq. 7 with stochastic optimization. Specifically, we use Monte Carlo approximations of the reparameterization gradient, a form of black box variational inference [Kingma and Welling, 2014, Ranganath et al., 2014]. Algorithm 2 summarizes this procedure. The complexity of VI-BIP is $O(T \cdot M \cdot c(\mathcal{D}, p))$ for T iterations and M gradient samples. When the cost of exact BIP inference is prohibitive, VI-BIP provides a good alternative.

A technical challenge in VI-BIP is computing gradients of the ELBO, which involve expectations with respect to the discrete variational distribution $q_\phi(z)$. Standard reparameterization gradients do not directly apply, as they require continuous latent variables. Here we use the unbiased U2G gradient estimator [Yin et al., 2020]; see Algorithm 3 in the supplementary materials. For a comprehensive discussion of gradient estimation methods for discrete latent variables, also see Mohamed et al. [2020]. Additional implementation and optimization details for VI-BIP are provided in Supplementary Section B.2.

3 Theory

We analyze asymptotic behavior of the posterior distribution $\hat{p}(z | \mathcal{D})$ obtained via exact inference (under estimated models \hat{p}_e) as described in Algorithm 1. For simplicity (and without loss) we assume the sample size is the same across environments, i.e. $n_e = n$. To enable asymptotic analysis of infinite environments, we assume each environment is drawn from a uniform distribution $p(e)$ over the set of all environments of interest \mathcal{E} .

We outline our theoretical findings as follows:

- § 3.1: Under suitable assumptions the posterior $\hat{p}(z \mid \mathcal{D})$ concentrates on the true z^* as both environment size E and per-environment sample size n grow to infinity. With additional regularity conditions, it contracts exponentially in n and E , with faster rates under stronger prior knowledge and greater environment heterogeneity.
- § 3.2: We extend the main results to settings with finite n or E . Additionally, we show that when assumptions are relaxed, the posterior concentrates on the most “approximately invariant” feature selectors under the given model and prior.

We use \xrightarrow{P} to denote convergence in probability, and $\forall_p z$ to mean for every z with positive prior value. Additional results and proofs are included in Supplementary Section A.

3.1 Main results

We make the following assumptions:

Assumption 2 (Uniqueness). *In Assumption 1, the existence of z^* is unique.*

Assumption 3 (Prior positivity). *In Assumption 1, z^* has positive prior mass.*

Assumption 4 (Estimation consistency). $\forall_p z$, as $n \rightarrow \infty$ and $E \rightarrow \infty$,

$$\begin{aligned} & \frac{1}{nE} \sum_{i=1}^n \sum_{e=1}^E \log \hat{p}_e(y_{ei} \mid x_{ei}^z) \xrightarrow{P} \mathbb{E}_{p(e)p_e(y, x^z)} [\log p_e(y \mid x^z)], \\ \text{and } & \frac{1}{nE} \sum_{i=1}^n \sum_{e=1}^E \log \hat{g}(y_{ei} \mid x_{ei}^z) \xrightarrow{P} \mathbb{E}_{p(e)p_e(y, x^z)} [\log g(y \mid x^z)]. \end{aligned}$$

With these assumptions, we now state our first theorem. Given infinite data and environments, BIP correctly identifies the invariant z^* .

Theorem 1 (Posterior consistency). *Suppose Assumptions 1 to 4 hold, and take the limits $n \rightarrow \infty$ and $E \rightarrow \infty$. The BIP posterior satisfies the following properties:*

- *consistency of the posterior mode: $\hat{z}_{n,E} := \arg \max_z \hat{p}(z \mid \mathcal{D}) \xrightarrow{P} z^*$*

- *consistency of the posterior at z^* : $\hat{p}(z^* | \mathcal{D}) \xrightarrow{P} 1$.*

The proof is provided in Supplementary Section A.2. Theorem 1 relies on key assumptions: Assumption 1 asserts that the true data generating process satisfies invariance; Assumption 2 guarantees identifiability of z^* ; Assumption 3 requires the prior is well-specified; Assumption 4 ensures consistent estimation of the likelihood.

Next, we characterize the posterior contraction rate. First we make an assumption.

Assumption 5 (Finite variance of log-likelihood ratio). $\forall_p z$, the log-likelihood ratio $\log p_e(y | x^z) - \log g(y | x^z)$ has finite variance, that is,

$$v(z) := \text{Var}_{p(e)p_e(y, x^z)} ([\log p_e(y | x^z) - \log g(y | x^z)]) < \infty.$$

This regularity condition enables control over posterior contraction through Chebyshev's inequality. To state the contraction rate, we define the total variational distance $\text{TV}(\cdot, \cdot)$ between the posterior and the Dirac measure centered at the true z^* as follows,

$$\text{TV}(\hat{p}(z | \mathcal{D}), \delta_{z^*}(z)) = \frac{1}{2} \left(\sum_{z \neq z^*} |\hat{p}(z | \mathcal{D}) - 0| + |p(z^* | \mathcal{D}) - 1| \right) = 1 - \hat{p}(z^* | \mathcal{D}).$$

Theorem 2 (Posterior contraction rate). *Given Assumptions 1 to 5, there exists a sequence $\epsilon_{n,E} = O(R \cdot e^{-\kappa n E \mu_{\min}})$ such that*

$$P \left(\text{TV}(\hat{p}(z | \mathcal{D}), \delta_{z^*}(z)) > \epsilon_{n,E} \right) \rightarrow 0$$

as $n \rightarrow \infty$ and $E \rightarrow \infty$, where κ is a fixed value in $(0, 1)$, and

$$R = \left(\max_{z \neq z^*} \frac{p(z)}{p(z^*)} \right) \cdot |\text{supp}(p(z))|, \quad (8)$$

$$\mu(z) := \mathbb{E}_{p(e)p_e(x^z)} [\text{KL}[p_e(y | x^z) \| g(y | x^z)]], \quad (9)$$

$$\mu_{\min} := \min_{z \neq z^*, z \in \text{supp}(p(z))} \bar{\mu}(z). \quad (10)$$

The proof is provided in Supplementary Section A.3. Theorem 2 shows that the BIP

posterior contracts around z^* exponentially fast, with respect to n and E . It also reveals two key factors that influence the contraction rate.

The first is the prior, which influences the term R in Eq. 8. An informative prior that assigns lower probability to non-invariant z s will lead to a smaller value of $\max_{z \neq z^*} \frac{p(z)}{p(z^*)}$ (or $|\text{supp}(p(z))|$), and hence a smaller R and faster contraction. In contrast, a prior fully supported on $\{0, 1\}^p$ results in an exponential dependence of R on the dimensionality p , since $|\text{supp}(p(z))| = 2^p$. This analysis highlights the challenge of high-dimensional invariant prediction problems and the importance of an informative prior in that setting.

The second factor is the heterogeneity of environments, captured by μ_{\min} in Eq. 10. μ_{\min} is defined as the minimum of $\mu(z)$ (Eq. 9) among non-invariant z s, where each $\mu(z)$ measures the discrepancy between local and pooled conditionals given z . By Assumption 1, $\mu(z^*) = 0$ and $\mu(z) > 0$ for $z \neq z^*$. When environments are more similar, local conditionals $p_e(y | x^z)$ tend to align and hence closer to the pooled conditional $g(y | x^z)$, yielding smaller $\mu(z)$. As a result, μ_{\min} is smaller, and the posterior contracts more slowly. Conversely, a larger μ_{\min} suggests greater environment heterogeneity, leading to faster posterior contraction. We empirically confirm this relationship in § 4.1, where we manually increase the environment heterogeneity level and observe faster contraction.

3.2 Finite-sample extensions and violations of the assumptions

We presented our main theoretical results with infinite samples per environments *and* infinite environments. Here, we consider several extensions, including finite-sample situations and cases where assumptions are violated. The detailed theorems and proofs are in Appendices A.4 and A.5. Here we summarize the main findings.

First, consider finite samples. Suppose we observe a fixed set of environments and per-environment sample size $n \rightarrow \infty$. The consistency results and rates from Section 3.1 continue to hold, provided that z^* remains identifiable within the observed environments. This condition requires sufficient heterogeneity among environments.

Alternatively, when each environment has finite samples but the number of environ-

ments grows large ($E \rightarrow \infty$), the local models $\hat{p}_e(y \mid x^z)$ become biased. We must control these biases for the consistency results to extend.

Now we consider violations of the main assumptions.

- *Violation of invariance (Assumption 1).* Recall the discrepancy measure $\mu(z)$ in Eq. 9. If invariance holds exactly, $\mu(z)$ reaches its minimum at z^* , with zero discrepancy $\mu(z^*) = 0$. When invariance is violated, the posterior concentrates on the feature selector minimizing $\mu(z)$, which is considered the most approximately invariant solution.
- *Violation of uniqueness (Assumption 2).* When multiple invariant feature selectors exist, the posterior distributes its mass among all invariant solutions. This issue is amplified with limited environments, while introducing additional environments reduces the number of posterior modes. § 4.2 provides an empirical illustration.
- *Violation of positive prior support (Assumption 3).* Suppose the prior assigns zero probability to the true invariant feature selector z^* . Then the posterior again concentrates on the most approximately invariant feature selector within the prior support.
- *Model misspecification (Assumption 4).* Suppose the estimation consistency assumption fails. Then the posterior concentrates on the minimizer of an alternative discrepancy measured (as opposed to $\mu(z)$ in Eq. 9), which captures the expected difference between the best-fitting local and pooled models within the assumed model class.

In sum, when assumptions hold exactly, the posterior is consistent for the true invariant features. When assumptions fail, it remains consistent, but toward the most approximately invariant features that are feasible within the model class and prior.

4 Synthetic study

We evaluate the BIP framework with simulated data under known distributions. With these simulations, we confirm our theory, explore the properties of uncertainty quantification, and empirically compare our approach to existing methods for invariant estimation.

In what follows, BIP as a standalone method refers to the version with exact inference, and VI-BIP denotes its variational approximation. All experimental details are provided in Supplementary Section C. We summarize our findings as follows:

- In § 4.1 we empirically verify the theory with $p = 3$ features where exact inference for BIP is tractable. Our results confirm posterior consistency and contraction rates as the number of environments E and per-environment sample size n increase.
- In § 4.2 we demonstrate how the BIP posterior quantifies uncertainty when there are multiple invariant sets, limited environments, and $p = 2$ features. We show how a multi-modal posterior empirically favors sparser feature selectors. As more environments are observed, the number of posterior modes decreases and the posterior uncertainty shrinks. This study supports the theory in § 3.2.
- In § 4.3 we compare BIP and VI-BIP to existing methods for invariant estimation. We study both a low-dimensional setting ($p = 10$) and high-dimensional setting ($p = 450$). We show that BIP and VI-BIP recover the invariant feature selector in low dimensions; and for high-dimensions, VI-BIP is more scalable and accurate than existing methods, while BIP with exact inference becomes computationally infeasible.

Data generation. To simulate multi-environment data, we specify a series of joint distributions that factorize consistently across environments:

$$p_e(x, y) = \prod_{i=1}^{p+1} p_e(t^{(i)} \mid t^{(1:i-1)}), \quad \forall e, \quad (11)$$

where the vector $t \in \mathbb{R}^{p+1}$ is a permuted version of the concatenated vector $(x^{(1:p)}, y)$. The permutation is drawn once and fixed across all environments.

Each conditional distribution in Eq. 11 is a linear Gaussian. For $i > 1$,

$$p_e(t^{(i)} \mid t^{(1:i-1)}) = \mathcal{N}(t^{(i)} \mid \alpha_{ei}^\top t^{(1:i-1)} + \beta_{ei}, \sigma_{ei}^2),$$

with parameters $\alpha_{ei} \in \mathbb{R}^{i-1}, \beta_{ei}, \sigma_{ei} \in \mathbb{R}$. For $i = 1$ we set $p_e(t^{(1)} \mid t^{(1:0)}) = \mathcal{N}(t^{(1)} \mid \beta_{e1}, \sigma_{e1}^2)$ with parameters $\beta_{e1}, \sigma_{e1} \in \mathbb{R}$. (For convenience, $t^{(1:0)}$ denotes an empty vector.)

We generate the parameters of these conditionals for the different environments as follows. For the *observational environment* ($e = 1$), we independently draw the parameter values $\{\alpha_{1i}, \beta_{1i}, \sigma_{1i}\}$ for each of the p features and the outcome, where $i = 1, \dots, p+1$. For the subsequent *interventional environments* ($e > 1$), we intervene on a subset of features based on the observational environment. Specifically, we draw an *intervention set* of features $x_{\mathcal{I}} \subset x$ and modify their conditional distributions. For non-intervened features $t^{(i)} \notin x_{\mathcal{I}}$, we retain the same conditional as in the observational environment, $p_e(t^{(i)} \mid t^{(1:i-1)}) = p_1(t^{(i)} \mid t^{(1:i-1)})$. For intervened features $t^{(i)} \in x_{\mathcal{I}}$, we independently draw new values $\{\alpha_{ei}, \beta_{ei}, \sigma_{ei}\}$ for each environment $e > 2$. Per the assumptions, the conditional distribution for the outcome y is invariant across all environments. This setup ensures distinct joint distributions $p_e(x, y)$ across environments, while the conditional outcome distribution $p(y \mid x^{z^*})$ remains invariant. To control the diversity of the environments, we also modulate the *intervention strength*, the fraction of intervened features $|x_{\mathcal{I}}|/p$.

Prior specification and model estimation With low-dimensional data ($p = 2, 3, 10$) we use a uniform prior of z over $\{0, 1\}^p$. With high-dimensional data ($p = 450$) we use a sparse prior. In all settings, we model local and pooled conditionals as linear Gaussians and estimate parameters via maximum likelihood estimation (Eq. 4 and Eq. 5, respectively). We use linear Gaussian models for competing methods as well.

4.1 Empirical verification of theory

We study the empirical behavior of the posterior in simulations with $p = 3$ features. We vary per-environment sample size n from 10 to 200, the number of environments E from 1 to 5, and intervention strength from 0.33 to 1 (intervening on 1 to 3 features).

Figure 1 (A) shows the posterior value at the true z^* , $\hat{p}(z^*|\mathcal{D})$. For each level of intervention strength, $\hat{p}(z^*|\mathcal{D})$ converges to 1 with increasing n or E , corroborating the theory on posterior consistency in § 3.1. The empirical rate at which $\hat{p}(z^*|\mathcal{D})$ converges

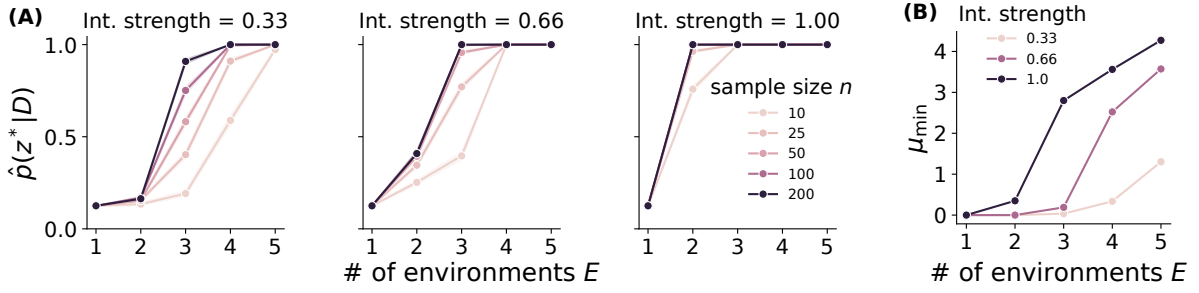


Figure 1: Synthetic study: empirical verification of posterior consistency (left) and contraction rate (right) with $p = 3$ features. **(A)**: The posterior value at the invariant z^* , $\hat{p}(z^* | \mathcal{D})$, increases with the per-environment sample size n , number of environments E , and intervention strength “Int. strength”. Results are averaged over 1,000 simulations with 95% confidence bands. **(B)**: The heterogeneity measure μ_{\min} (Eq. 10), which controls the posterior contraction rate $\epsilon_{n,E} = O(R \cdot e^{-\kappa n E \mu_{\min}})$, increases with both the number of environments E as well as intervention strength.

to 1 is faster under higher intervention strength.

Figure 1 (B) plots the heterogeneity metric μ_{\min} that governs the posterior contraction rate $\epsilon_{n,E} = O(R \cdot e^{-\kappa n E \mu_{\min}})$ against the number of environments E under different intervention strength. We observe that μ_{\min} increases with both E and intervention strength. In both cases, the observed environments become more heterogeneous, leading to faster posterior contraction. The trend in Figure 1 (B) aligns with the empirical trend in Figure 1 (A), confirming the expected posterior contraction behavior.

4.2 Uncertainty quantification in limited environments

We present a synthetic example in which multiple invariant feature selectors exist under a limited number of environments, supporting the discussion in § 3.2.

We construct 3 environments with $p = 2$ features, $x = [x^{(1)}, x^{(2)}]$, with following properties: (A) $p_e(y | x^{(1)})$ and $p_e(y | x^{(1:2)})$ are invariant across $e = 1, 2$; (B) After introducing the third environment, only $p_e(y | x^{(1)})$ remains invariant. For each environment, we draw $n = 200$ samples. Supplementary Section C.2 gives the details of this data.

Figure 2 plots the posterior distribution for all four possible z values. With only two environments (left panel), the posterior is multimodal, placing substantial mass on $z = [1, 0]$ and $z = [1, 1]$. After introducing the third environment (right panel), the posterior concentrates only at $z = [1, 1]$ and the uncertainty shrinks accordingly. This result

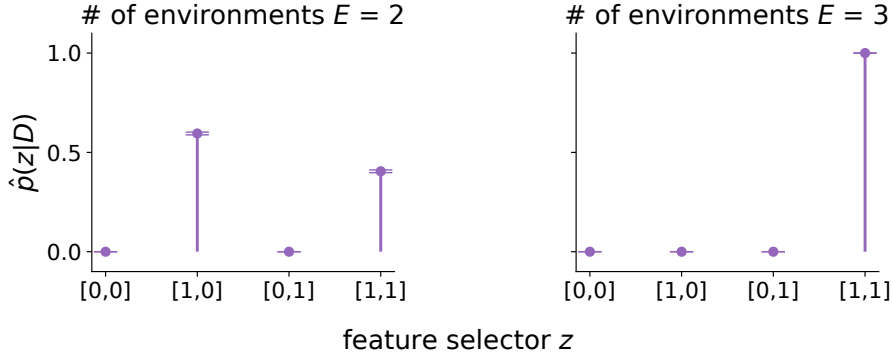


Figure 2: Synthetic study: uncertainty quantification with $p = 2$ features. Given $E = 2$ environments (left), the posterior $\hat{p}(z | \mathcal{D})$ is multi-modal, centered at two invariant solutions $z = [1, 0], [1, 1]$. When a new environment is introduced ($E = 3$, right), $z = [1, 0]$ becomes the only invariant feature selector. The updated posterior is only concentrated at $[1, 0]$. All results are averaged over 1,000 simulations with 95% confidence bands.

supports the discussion in § 3.2: sufficiently heterogeneous environments are necessary for posterior consistency, whereas with limited environments, the posterior concentrates on all valid invariant selectors.

Finally, we note that with two environments (Figure 2, left panel), the posterior density at $z = [1, 0]$ is higher than that at $z = [1, 1]$, despite both yielding invariant predictions. This difference arises from model estimation bias: estimating conditional models given two features ($z = [1, 1]$) typically results in a larger estimation bias, compared to models given one feature ($z = [1, 0]$), and especially so for small sample sizes. When true models are available, this estimation artifact disappears—with large sample sizes (and a uniform prior), the posterior assigns equal mass to both solutions.

4.3 Comparison to other methods

We now compare BIP and VI-BIP to existing methods for invariant estimation. Here we present the main results. Supplementary Section C.3 contains additional details and results.

Empirical setup. We perform separate simulations with feature sizes $p = 10$ and $p = 450$. We vary the per-environment sample size n from $\{50, 200, 500\}$, and vary the number of environments E from 1 to 20 for $p = 10$, and from 1 to 40 for $p = 450$. For each combination of (p, n, E) , we generate 400 datasets under different intervention strengths.

With this catalog of simulations, we compare the following methods:

1. *Oracle*: We fit a pooled linear regression on the true invariant features x^{z*} and return the ones significant at the $\alpha = 0.05$ level. If $p + 1 > nE$, we use Lasso with 10-fold cross-validation and return the top 10 features by absolute coefficient values.
2. *Regression*: Similar to the oracle, but linear regression is performed on all features rather than restricting to the true invariant features.
3. *Invariant causal prediction (ICP)* [Peters et al., 2016]: With ICP, we use the significance level $\alpha = 0.05$ for its multiple hypothesis testing procedure.
4. *Hidden-ICP* [Rothenhäusler et al., 2019] An extension of ICP enabling faster inference for an alternative notion of invariance. We run it at the significance level $\alpha = 0.05$.
5. *EILLS* [Fan et al., 2023]: A linear regression model that introduces a regularization term to encourage invariant predictions among environments. Following the default choice in their codebase, the regularization penalty is set to 36.
6. *Bayesian invariant prediction (BIP)* [this paper]: Our method with exact inference (Algorithm 1). We use the posterior mode as the BIP estimate of the invariant selector.
7. *Variational inference BIP (VI-BIP)* [this paper]: Our method with variational inference (Algorithm 2). Again, we use the posterior mode as the VI-BIP estimate of the invariant selector. Supplementary Section B.2 provides more details about the optimization.

Note that BIP, ICP and EILLS require enumerating all candidate invariant sets, which is only feasible for small p . And for Hidden-ICP, parameter estimation is intractable when p exceeds the number of observations. To address these issues in the high dimensions ($p = 450$), we first apply a screening step, selecting the 10 features with the largest absolute regression coefficients. We then apply the methods that cannot handle the full dimension to only the screened features. In the results, we label these screened versions of the algorithms as *BIP-s*, *ICP-s*, *Hidden-ICP-s*, and *EILLS-s*.

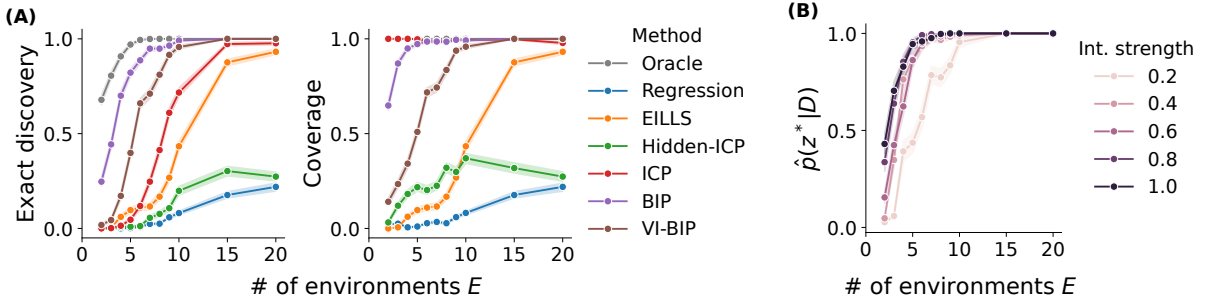


Figure 3: Synthetic study: comparison to other methods with $p = 10$ features. Results are averaged over cases with $n = 50, 200, 500$, each with 400 random simulations under varying intervention strength. Error bars indicate 95% confidence intervals. **(A)**: Exact discovery rate improves with E for all methods, with Oracle converging fastest, followed by BIP and VI-BIP. Oracle and ICP maintain coverage near 1 across all E , while coverage for BIP, VI-BIP, and ELLIS gradually increases to 1. Other methods show relatively low coverage. **(B)**: BIP’s posterior value at z^* increases with both E and intervention strength, as each case leads to higher heterogeneity across environments.

We emphasize that VI-BIP does not require enumeration of candidate sets, and so more easily applies to high-dimensional settings. However, we found that the uniform prior over the full space of $\{0, 1\}^p$ leads to unstable optimization when p is large. In the high dimensional case ($p = 450$), we set the prior to be uniform over $\{z \in \{0, 1\}^p : \|z\|_0 \leq 20\}$, i.e., a uniform prior over sets of 20 features. Note we still optimize over all sets of 20 features. This informative prior is significantly different from a screening step.

Evaluation metrics. Each method produces an estimate of the invariant selector \hat{z}^* . Given the ground truth z^* , we use two metrics: (i) *exact discovery rate*, which measures the average occurrence where the estimated invariant features exactly recover the true invariant features, and (ii) *coverage*, which measures the average occurrence where the estimated invariant features is a subset of the true invariant features. A perfect method should achieve 1 on both metrics. We emphasize that coverage alone can be misleading, as always predicting the empty set yields full coverage but zero exact discovery.

Low-dimensional results. Figure 3 displays the results for $p = 10$. Panel (A) plots the exact discovery rate (left) and coverage (right) versus the number of environments E . As E increases, all methods improve in exact discovery rate. At $E = 20$, all except Regression and Hidden-ICP reach an exact discovery rate close to 1, demonstrating effectiveness with sufficient environments. Oracle converges fastest, followed by BIP and VI-BIP.

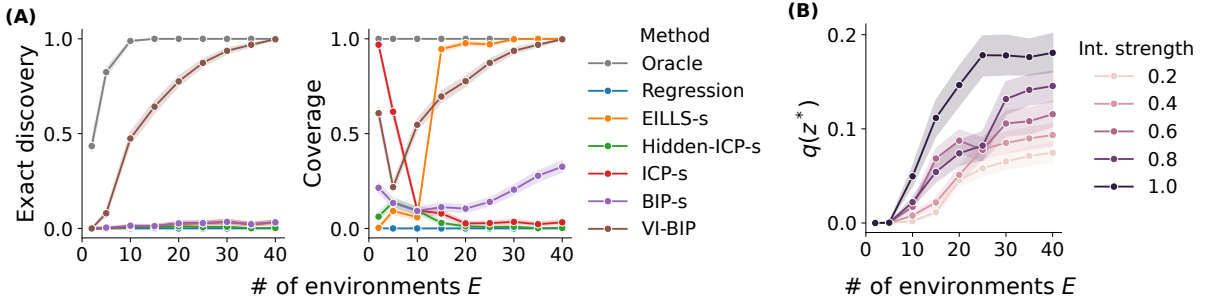


Figure 4: Synthetic study: comparison to other methods with $p = 450$ features. Results are averaged over cases with $n = 50, 200, 500$, each with 400 random simulations under varying intervention strength. Error bars indicate 95% confidence intervals. Methods with the “-s” suffix use a pre-screening step. **(A)**: The exact discovery rate of Oracle and VI-BIP converges to 1 as E increases, while it remains low for other methods. Oracle maintains near-perfect coverage across all E , and coverage of VI-BIP gradually approaches to 1. EILLS-s achieves high coverage at large E but this is due to frequent empty predictions. Other methods have low coverage. **(B)**: the variational posterior value at the true z^* by VI-BIP increases with both E and intervention strength, but remains below 0.2 even at the largest $E = 40$ considered.

For coverage, we observe an upward trend for all methods as E increases. Both the oracle and ICP consistently maintain a coverage close to 1 across different values of E . Notably, when E is small, ICP returns empty prediction for most simulations, leading to a high coverage but low exact discovery rate. The coverage of our methods, both BIP and VI-BIP, converges to near perfect coverage when $E = 20$.

Figure 3 (B) displays the posterior value at the true z^* given by BIP. The posterior value converges to 1 with more environments. Additionally, the convergence is faster with higher intervention strength. This result is consistent with the theoretical contraction rates. We include the variational posterior value at z^* from VI-BIP in Figure S3 in the supplementary material, where we observe a similar trend as in the exact inference, but with a slower convergence rate compared to the exact posterior.

High-dimensional results. Figure 4 gives the results for $p = 450$. Panel A (Left) shows the exact discovery rate of the oracle and VI-BIP converges to 1 as E increases. In contrast, the remaining methods exhibit a near-zero exact discovery rate across E , primarily due to failures in the pre-screening step.

Panel (A) also displays the coverage results. As expected, the gold-standard oracle maintains near-perfect coverage. The coverage of VI-BIP approaches 1 as more environ-

ments are observed. Notably, EILLS achieves high coverage at large E by predicting an empty invariant feature set in these scenarios. The remaining methods have low coverage.

Figure 4 (B) plots the variational posterior density $q(z^*)$ at the true z^* by VI-BIP. $q(z^*)$ increases with larger E or higher intervention strength. However, $q(z^*)$ is not close to 1 even at the largest $E = 40$ tested, reflecting a sufficient amount of uncertainty. This uncertainty amplifies the marginal uncertainty in the mean-field variational distribution. For example, if each marginal $q(z^{*(i)}) = .996, \forall i$, then the joint posterior value is exponentially smaller $q(z^*) = .996^{450} = .165$, leading to substantial overall uncertainty.

5 Gene perturbation study

We revisit a real-world application studied in [Peters et al. \[2016\]](#), [Meinshausen et al. \[2016\]](#), [Rothenhäusler et al. \[2019\]](#) which involves predicting genes whose deletion significantly alters the expression of some target gene. All experimental details are provided in Supplementary Section D. Our findings are summarized below.

- VI-BIP achieves high precision and moderate recall, outperforming existing invariant prediction approaches that depend on feature pre-screening in high dimensions.
- VI-BIP’s predictions closely align with the top 10 stable findings reported in [Meinshausen et al. \[2016\]](#).

Dataset and setup. The dataset comes from a large-scale gene perturbation experiment in yeast, where genome-wide mRNA expression levels are measured for 6,170 genes [[Kemmeren et al., 2014](#)]. It includes two environments: 262 observational samples for $e = 1$ where no gene deletion is performed, and 1,479 interventional samples for $e = 2$ where each sample is obtained by a unique gene deletion. Our goal is to predict whether an unseen gene deletion will significantly change the expression level of some target gene.

Following [Peters et al. \[2016\]](#), this problem can be approached by invariant prediction. We treat the expression level of the target gene as outcome y and the expression levels of

the remaining $p = 6,169$ genes as features x . The goal becomes to find a subset of feature genes $x^{z^*} \subset x$ that invariantly predict y across environments. If an invariant feature $x' \in x^{z^*}$ is perturbed, then the outcome y is expected to change in a new environment created by this perturbation, which allows us to predict the effect of an gene prediction. For non-invariant feature $x' \notin x^{z^*}$, we do not make such prediction. [Peters et al. \[2016\]](#) also provides a justification through a causal perspective, where the invariant feature genes are viewed as the direct causes of the target gene.

We set up the training and validation procedure largely following [Peters et al. \[2016\]](#). The interventional samples from $e = 2$ are randomly divided into 5 blocks at the beginning. We then sweep through 6,170 genes, treating each as the target gene, with the remaining genes as features. For each target gene, we construct a training set that includes all observational samples from $e = 1$ and 4 out of 5 blocks of interventional samples from $e = 2$, reserving the remaining block for validation. Note if the training set contains a sample corresponding to the perturbation of the target gene, we exclude it as we want to make sure the distribution of the target gene is not affected. This process is repeated five times, with each block of interventional samples held out once, ensuring that each gene perturbation result is used for validation at least once. To evaluate predictions of invariant features, we check the validation set to determine whether perturbing these features leads to a significant change in the expression level of the target gene.

We run the following methods to infer the invariant feature selector z^* :

1. *Marginal*: we pool training data over the two environments and retain all features that have a correlation with the outcome y at significance level α/p with $\alpha = 0.01$.
2. *Lasso*: we run Lasso on the pooled training data where the regularization penalty is selected from $\{0.1, 0.05, 0.01, 0.005, 0.001\}$ with 5-fold cross-validation and retain up to 10 features with the highest non-zero absolute coefficient values.
3. *EILLS-s* [[Fan et al., 2023](#)]: we run EILLS on the screened features with an invariance regularization strength γ . We vary $\gamma \in \{1, 25, 50, 75, 100\}$;

4. *Hidden-ICP-s* [Rothenhäusler et al., 2019]: We run hidden-ICP on the screened covariates at significance level α . We vary $\alpha \in \{0.001, 0.005, 0.01, 0.05, 0.1\}$;
5. *ICP-s* [Peters et al., 2016]: we run ICP on the screened features at significance level α/n_{int} . We vary $\alpha \in \{0.001, 0.005, 0.01, 0.05, 0.1\}$, and the factor $n_{int} = 1,479$ is used for Bonferroni correction, as suggested by Peters et al. [2016].
6. *BIP-s* [this paper]: we calculate the exact BIP posterior using the screened features with a uniform prior, retaining features whose marginal posterior probability is above a threshold t . We vary $t \in \{0.5, 0.6, 0.7, 0.8, 0.9\}$.
7. *VI-BIP* [this paper]: we run VI-BIP using the full set of features with a sparse prior uniform over $\{z \in \{0, 1\}^p : \|z\|_0 \leq 200\}$, retaining the features whose marginal posterior probability is above a threshold t . We vary $t \in \{0.5, 0.6, 0.7, 0.8, 0.9\}$. See the optimization details in Supplementary Section D.

As in the synthetic study, EILLS-s, ICP-s, BIP-s and Hidden-ICP-s all use a pre-screening step due to high dimensionality. The screened features are initially selected using the features returned by Lasso. If Lasso does not return any features (all coefficients are 0) we instead select up to the top 10 features with largest absolute correlation values from Marginal. For all methods, the conditional outcome distribution is a linear Gaussian.

Evaluation metrics. To compare the methods, we measure *precision* and *recall*. We evaluate the effect of a predicted invariant feature gene on the target gene using a held-out validation set. If deleting the feature gene leads to a significant change in the expression level of the target, the prediction is considered correct.

Due to the limited validation data, not all predictions can be empirically validated. Therefore, we compute *precision* as the ratio of correct predictions to the total number of predictions that can be validated. Similarly, *recall* is the ratio of the correct predictions to the total number of significant gene deletion effects that can be validated.

Results. Figure 5 presents the results, excluding *Marginal* as it is an outlier. Different methods demonstrate different trade-offs between precision and recall. We summarize

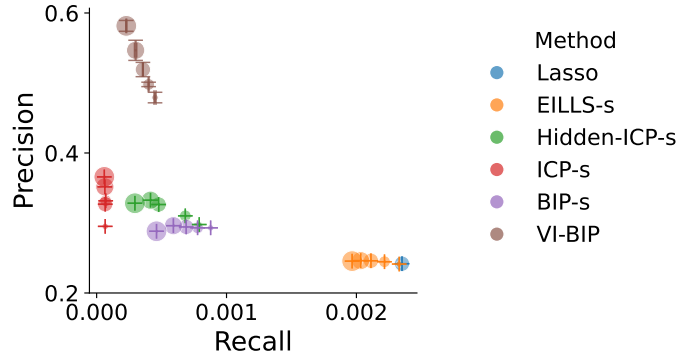


Figure 5: Gene perturbation study: precision v.s. recall. Each dot shows the average result over 3 random seeds, with error bars indicating 2 standard errors. Colors denote methods, and multiple dots per method reflect different hyperparameter settings with larger dots indicating more conservative settings (see Supplementary Section D). VI-BIP consistently achieves a favorable precision-recall trade-off with the highest precision among all methods and recall higher than ICP-s across different hyperparameter settings.

as follows: (i) VI-BIP is the most accurate method (with highest precision) and has a moderate recall; (ii) ICP-s is the second most accurate but also the most conservative as indicated by the lowest recall; (iii) Other invariant prediction methods and Lasso have lower precision and higher recall compared to VI-BIP; (iv) Marginal, which is not plotted in the figure, has the lowest precision of 0.11, but the highest recall of 0.87. These patterns remain consistent across the range of hyperparameter settings used for each method.

We discuss potential reasons why Marginal exhibits significantly higher recall values than the other methods. For methods that rely on screening, lower recall is expected as their predictions are constrained within a maximum of 10 screened features. VI-BIP, while it does not use screening, imposes a sparse prior with a maximum invariant feature size of 200, which also restricts recall. Moreover, the true posterior, based on only two environments, may be multi-modal. In such cases, the mean-field variational distribution used by VI-BIP may struggle to capture the full posterior landscape, leading to partial coverage and thereby reduced recall. Other contributing factors include violations of the invariance assumption and misspecification of the conditional outcome model.

Comparison between VI-BIP and ICP-s. Finally, we provide a detailed comparison between VI-BIP and ICP-s, as they achieve higher precision than other methods. We examine the predictions made by VI-BIP with a marginal probability threshold of $t = 0.5$,

and by ICP-s with a significance level of $\alpha = 0.01$. For a fixed target gene, we take the intersection of predicted invariant feature sets across 3 random seeds per method. We find that approximately 42% (27 out of 67) of correct predictions by ICP-s are also identified by VI-BIP, suggesting some degree of consistency. Moreover, VI-BIP is less conservative than ICP-s, with a total of 371 correct predictions – about 5.5 times as many as ICP-s.

We also compare our findings with those of [Meinshausen et al. \[2016\]](#). They use ICP at a significance level of $\alpha = 0.01$ after a Lasso pre-screening procedure, followed by an additional stability selection step [[Meinshausen and Bühlmann, 2010](#)] applied to 50 randomly bootstrapped datasets. In addition, the dataset used in [Meinshausen et al. \[2016\]](#) only has 160 observational samples, whereas the updated version that we use has 262 observational samples ¹. Table 1 gives the results. Most of the verified effects predicted by VI-BIP, ICP-s, and [Meinshausen et al. \[2016\]](#) are the same.

6 Discussion and future works

We present *Bayesian Invariant Prediction (BIP)* to infer the subset of features that invariantly predict the outcome across diverse environments. For high-dimensional settings, we develop VI-BIP, a scalable variational algorithm that addresses the exponential complexity of exact inference. We establish theoretical guarantees on posterior consistency and derive posterior contraction rates that depend both on the amount of data and the heterogeneity of the environments. We validate BIP and VI-BIP in both synthetic and real data studies, demonstrating their accuracy, uncertainty quantification, and scalability.

The fundamental assumptions of BIP are that the multi-environment data generative process is truly invariant, and that the chosen model class accurately reflects the invariant prediction mechanism. When these conditions are met, BIP offers a principled way to identify invariant features and make predictions that are robust to distribution shifts across environments. In practice, when these assumptions may not hold exactly, BIP identifies the most approximately invariant feature set. These results remain valuable for

¹The updated dataset can be downloaded at <https://deleteome.holstegelab.nl/>.

interpreting the data through a simplified lens and identifying robust features.

BIP also offers a new perspective to invariant prediction in high dimensions. While previous methods often rely on feature pre-screening or additional regularization terms, our variational approach VI-BIP provides an optimization-based alternative. Our empirical results show that it achieves higher accuracy, and without being overly conservative.

One limitation BIP is that they rely on fixed estimates of per-environment distributions, and do not quantify uncertainty around them. In this work, we use maximum likelihood estimates and, as a result, the estimation bias can obscure the posterior inference especially with small sample size. Integrating conditional model estimation into the overall probabilistic framework is an important avenue of further research.

Another future direction is to explore more expressive conditional model classes and develop efficient training algorithms. While our method and theory apply generally, our experiments only considered linear Gaussian models (for computational convenience). Future work can consider richer model classes, combined with amortized computation.

Finally, VI-BIP uses a factorized mean-field variational family, which is effective and efficient, but may limit posterior expressiveness. A third future direction is to incorporate advances in variational inference and discrete variable optimization to improve VI-BIP.

Target gene	Inferred invariant feature gene(s)		
	Meinshausen et al. [2016]	ICP-s ($\alpha = 0.01$)	VI-BIP ($t = 0.5$)
YMR103C	YMR104C	YMR104C	YMR104C, YHR209W*
YMR321C	YPL273W	YPL273W	YPL273W
YCL042W	YCL040W	YCL040W	YCL040W
YLL020C	YLL019C	YLL019C	YLL019C
YPL240C	YMR186W	YMR186W	YJL077C, YMR186W
YBR126C	YDR074W	\emptyset	YGR008C*, YKL035W*, YDR074W
YMR173W-A	YMR173W	YMR173W, YOL100W*	YMR173W
YGR264C	YGR162W	\emptyset	\emptyset
YJL077C	YOR027W	\emptyset	YLL026W*, YOR027W, YFL010W-A*
YLR170C	YJL115W [×]	YDR322C-A*, YDR180W* YJL184W*, YLR438C-A*	\emptyset

Table 1: Invariant genes predicted by different methods: ICP from previous findings [Meinshausen et al., 2016] (left column); our implementation of ICP-s (middle column); and VI-BIP (right column). We observe consistency in most of their predictions on the 10 target genes selected by Meinshausen et al. [2016]. Genes in blue are validated to have significant effects on the corresponding target gene; genes marked with a superscript * cannot be checked given existing data. Genes with a superscript [×] can be checked but do not have a significant effect; \emptyset means no invariant features are predicted by the method.

References

- Jonas Peters, Peter Bühlmann, and Nicolai Meinshausen. Causal inference by using invariant prediction: Identification and confidence intervals. *Journal of the Royal Statistical Society Series B: Statistical Methodology*, 78(5):947–1012, 2016.
- Jianqing Fan, Cong Fang, Yihong Gu, and Tong Zhang. Environment invariant linear least squares. *arXiv preprint arXiv:2303.03092*, 2023.
- Peter Bühlmann. Invariance, causality and robustness. *Statistical Science*, 35(3):404–426, 2020.
- Mateo Rojas-Carulla, Bernhard Schölkopf, Richard Turner, and Jonas Peters. Invariant models for causal transfer learning. *Journal of Machine Learning Research*, 19(36):1–34, 2018.
- Martin Arjovsky, Léon Bottou, Ishaan Gulrajani, and David Lopez-Paz. Invariant risk minimization. *arXiv preprint arXiv:1907.02893*, 2019.
- M. Jordan, Z. Ghahramani, T. Jaakkola, and L. Saul. Introduction to variational methods for graphical models. *Machine Learning*, 37:183–233, 1999.
- David M Blei, Alp Kucukelbir, and Jon D McAuliffe. Variational inference: A review for statisticians. *Journal of the American statistical Association*, 112(518):859–877, 2017.
- Mingzhang Yin, Yixin Wang, and David M. Blei. Optimization-based causal estimation from heterogeneous environments. *Journal of Machine Learning Research*, 25(168):1–44, 2024.
- Dominik Rothenhäusler, Peter Bühlmann, and Nicolai Meinshausen. Causal Dantzig. *The Annals of Statistics*, 47(3):1688–1722, 2019.
- Patrick Kemmeren, Katrin Sameith, Loes AL Van De Pasch, Joris J Benschop, Tineke L Lenstra, Thanasis Margaritis, Eoghan O’Duibhir, Eva Apweiler, Sake van Wageningen,

- Cheuk W Ko, et al. Large-scale genetic perturbations reveal regulatory networks and an abundance of gene-specific repressors. *Cell*, 157(3):740–752, 2014.
- Jonas Peters, Dominik Janzing, and Bernhard Schölkopf. *Elements of Causal Inference: Foundations and Learning Algorithms*. The MIT Press, 2017.
- Bernhard Schölkopf, Francesco Locatello, Stefan Bauer, Nan Rosemary Ke, Nal Kalchbrenner, Anirudh Goyal, and Yoshua Bengio. Toward causal representation learning. *Proceedings of the IEEE*, 109(5):612–634, 2021.
- Ragnar Frisch, Trygve Haavelmo, Tjalling C. Koopmans, and Jan Tinbergen. *Autonomy of Economic Relations*. Memorandum fra Universitets Socialøkonomiske Institutt. Universitets Socialøkonomiske Institutt, Oslo, Norway, 1948.
- Kevin D. Hoover. Causality in economics and econometrics. In Steven N. Durlauf and Lawrence E. Blume, editors, *The New Palgrave Dictionary of Economics*. Palgrave Macmillan, Basingstoke, UK, 2nd edition, 2008.
- Judea Pearl. *Causality: Models, Reasoning, and Inference*. Cambridge University Press, New York, NY, 2nd edition, 2009.
- Christina Heinze-Deml, Jonas Peters, and Nicolai Meinshausen. Invariant causal prediction for nonlinear models. *Journal of Causal Inference*, 6(2):20170016, 2018.
- Zhenyu Wang, Yifan Hu, Peter Bühlmann, and Zijian Guo. Causal invariance learning via efficient optimization of a nonconvex objective. *arXiv preprint arXiv:2412.11850*, 2024.
- Yihong Gu, Cong Fang, Yang Xu, Zijian Guo, and Jianqing Fan. Fundamental computational limits in pursuing invariant causal prediction and invariance-guided regularization. *arXiv preprint arXiv:2501.17354*, 2025.
- D. Kingma and M. Welling. Auto-encoding variational Bayes. In *International Conference on Learning Representations*, December 2014.

- Rajesh Ranganath, Sean Gerrish, and David Blei. Black box variational inference. In *Artificial intelligence and statistics*, pages 814–822. PMLR, 2014.
- Mingzhang Yin, Nhat Ho, Bowei Yan, Xiaoning Qian, and Mingyuan Zhou. Probabilistic best subset selection via gradient-based optimization. *arXiv preprint arXiv:2006.06448*, 2020.
- Shakir Mohamed, Mihaela Rosca, Michael Figurnov, and Andriy Mnih. Monte Carlo gradient estimation in machine learning. *Journal of Machine Learning Research*, 21(132):1–62, 2020.
- Nicolai Meinshausen, Alain Hauser, Joris M Mooij, Jonas Peters, Philip Versteeg, and Peter Bühlmann. Methods for causal inference from gene perturbation experiments and validation. *Proceedings of the National Academy of Sciences*, 113(27):7361–7368, 2016.
- Nicolai Meinshausen and Peter Bühlmann. Stability selection. *Journal of the Royal Statistical Society Series B: Statistical Methodology*, 72(4):417–473, 2010.
- Leslie N Smith. Cyclical learning rates for training neural networks. In *2017 IEEE winter conference on applications of computer vision (WACV)*, pages 464–472. IEEE, 2017.
- A Paszke. Pytorch: An imperative style, high-performance deep learning library. *arXiv preprint arXiv:1912.01703*, 2019.

Supplementary Material

A Additional Theory and Proofs

In this section we provide additional theoretical results and proofs that are in complement to § 3.

Notation. We write $\forall_p a$ to mean “for $p(a)$ -almost every realization of a ” for a random variable (a) a probability measure $p(a)$.

A.1 Preliminary lemmas

We first introduce two lemmas that are helpful for proofs of the main theorems.

Lemma 1. *Let $\{X_n\}$ be a sequence of random variables where each $X_n \in \mathbb{R}^p$ and p is a fixed number. Assume $X_n \xrightarrow{P} \mu$ for some constant $\mu \in \mathbb{R}^p$, and define $\mathcal{I}^* := \{i : \mu_i = \mu_{\max}\}$ where μ_{\max} is value of the largest component(s) of μ and therefore \mathcal{I}^* is the set of corresponding indices. Let $i_n^* := \arg \max_i X_n^{(i)}$ denote the index of the maximal component of X_n . Then we have*

$$P(i_n^* \in \mathcal{I}^*) \rightarrow 1, \text{ as } n \rightarrow \infty.$$

As a special case, when $\mathcal{I}^ = \{i^* : \mu_{i^*} > \mu_j \forall j \neq i^*\}$ is a singleton, we have*

$$i_n^* \xrightarrow{P} i^*, \text{ as } n \rightarrow \infty.$$

Proof By continuous mapping theorem, $\forall j \notin \mathcal{I}^*$, as $n \rightarrow \infty$,

$$\max_{i \in \mathcal{I}^*} X_n^{(i)} - X_n^{(j)} \xrightarrow{P} \mu_{\max} - \mu^{(j)} > 0.$$

Hence $P(\max_{i \in \mathcal{I}^*} X_n^{(i)} - X_n^{(j)} < 0) \rightarrow 0$ as $n \rightarrow \infty$.

Consequently, as $n \rightarrow \infty$,

$$P(i_n^* \notin \mathcal{I}^*) = P(\exists j \notin \mathcal{I}^*, \max_{i \in \mathcal{I}^*} X_n^{(i)} < X_n^{(j)}) \leq \sum_{j \notin \mathcal{I}^*} P(\max_{i \in \mathcal{I}^*} X_n^{(i)} - X_n^{(j)} < 0) \rightarrow 0,$$

and therefore

$$P(i_n^* \in \mathcal{I}^*) \rightarrow 1.$$

■

Lemma 2. *Let $\{X_n\}$ be a sequence of random variables such that its sample average $\frac{S_n}{n}$ converges to some constant μ in probability, where $S_n := \sum_{i=1}^n X_i$. When $\mu < 0$, Then we have*

$$\exp\{S_n\} \xrightarrow{P} 0.$$

And when $\mu > 0$, we have

$$\exp\{S_n\} \xrightarrow{P} \infty.$$

Proof

Suppose $\mu < 0$. $\forall \epsilon > 0, \forall \delta > 0$, it suffices to find an $N = N(\epsilon, \delta)$ such that for $n > N$,

$$P(\exp\{S_n\} < \epsilon) = P\left(\frac{S_n}{n} < \frac{1}{n} \log \epsilon\right) > 1 - \delta.$$

Since $\frac{S_n}{n} \xrightarrow{P} \mu$, for $\epsilon' = -\frac{\mu}{2}$ and δ given above, $\exists N' = N'(\epsilon', \delta)$ such that for $n > N'$,

$$P\left(\frac{S_n}{n} < \mu + \epsilon'\right) > 1 - \delta.$$

We choose $N = \max(N', \frac{1}{\mu + \epsilon'} \log \epsilon)$. For $n > N$, we have

$$\frac{1}{n} \log \epsilon > \mu + \epsilon',$$

and therefore

$$P\left(\frac{S_n}{n} < \frac{1}{n} \log \epsilon\right) > P\left(\frac{S_n}{n} < \mu + \epsilon'\right) > 1 - \delta.$$

Next, we consider $\mu > 0$. $\forall \delta > 0, M > 0$, it suffices to find an $N = N(M, \delta)$ such that for $n > N$,

$$P(\exp\{S_n\} > M) = P(S_n > \log M) > 1 - \delta.$$

Since $\frac{S_n}{n} \xrightarrow{P} \mu$, for $\epsilon' = \frac{\mu}{2}$ and δ given above, $\exists N' = N'(\epsilon', \delta)$ such that

$$P\left(\frac{S_n}{n} > \mu - \epsilon'\right) > 1 - \delta.$$

We choose $N = \max(N, \frac{1}{\mu - \epsilon'} \log M)$. For $n > N$, we have

$$n(\mu - \epsilon') > \log M$$

and therefore

$$P(S_n > \log M) > P(S_n > n(\mu - \epsilon')) > 1 - \delta.$$

■

Lemma 3. Recall definition of $\mu(z)$ in Eq. 9:

$$\mu(z) = \mathbb{E}_{p(e)p_e(x^z)} [\text{KL} [p_e(y \mid x^z) \parallel g(y \mid x^z)]] .$$

We have

$$\mu(z) = 0 \Leftrightarrow p_e(y \mid x^z) \text{ is invariant with respect to } e \quad \forall_p e \forall x^z$$

Proof By the property of KL divergence, we have

$$\begin{aligned} \mu(z) = 0 &\Leftrightarrow \text{KL}[p_e(y \mid x) \parallel g(y \mid x^z)] = 0 \quad \forall_p e \forall x^z \\ &\Leftrightarrow p_e(y \mid x^z) = g(y \mid x^z) \quad \forall_p e \forall x^z \\ &\Leftrightarrow p_e(y \mid x^z) \text{ is invariant to } e \quad \forall_p e \forall x^z \end{aligned}$$

■

A.2 Proof of Theorem 1

Theorem (Posterior consistency) (Restatement of Theorem 1). *Suppose Assumptions 1 to 4 hold, and take the limits $n \rightarrow \infty$ and $E \rightarrow \infty$. The BIP posterior satisfies the following properties:*

- consistency of the posterior mode: $\hat{z}_{n,E} := \arg \max_z \hat{p}(z \mid \mathcal{D}) \xrightarrow{P} z^*$
- consistency of the posterior at z^* : $\hat{p}(z^* \mid \mathcal{D}) \xrightarrow{P} 1$.

Proof The posterior in Eq. 6 can be re-written as

$$\hat{p}(z \mid \mathcal{D}) = \frac{p(z) \exp\{-\hat{S}_{n,E}(z)\}}{\sum_z p(z) \exp\{-\hat{S}_{n,E}(z)\}} \quad (12)$$

where $\hat{S}_{n,E}(z)$ is the log-likelihood ratio given z ,

$$\hat{S}_{n,E}(z) := \sum_{i=1}^n \sum_{e=1}^E \log \hat{p}_e(y_{ei} \mid x_{ei}^z) - \log \hat{g}(y_{ei} \mid x_{ei}^z). \quad (13)$$

By Assumption 4, as $n, E \rightarrow \infty$,

$$\frac{1}{nE} \hat{S}_{n,E}(z) \xrightarrow{P} \mathbb{E}_{p(e)p_e(y|x^z)} [\log p_e(y | x^z)] - \mathbb{E}_{p(e)p_e(y|x^z)} [\log g(y | x^z)].$$

Recall the definition of $\mu(z)$ in Eq. 9, the RHS reduces to $\mu(z)$ and hence

$$\frac{1}{nE} \hat{S}_{n,E}(z) \xrightarrow{P} \mu(z). \quad (14)$$

Applying Lemma 1, as $n \rightarrow \infty$ and $E \rightarrow \infty$

$$\arg \max_{z:p(z)>0} -\frac{1}{nE} \hat{S}_{n,E}(z) \xrightarrow{P} \arg \max_{z:p(z)>0} -\mu(z) = z^*,$$

where the last equality follows from Assumptions 2 and 3 and Lemma 3.

Consequently, the posterior mode is consistent:

$$\begin{aligned} \hat{z}_{n,E} &:= \arg \max_z \hat{p}(z | \mathcal{D}) \\ &= \arg \max_{z:p(z)>0} \log p(z) - \hat{S}_{n,E}(z) \\ &= \arg \max_{z:p(z)>0} \frac{1}{nE} \log p(z) - \frac{1}{nE} \hat{S}_{n,E}(z) \\ &= \arg \max_{z:p(z)>0} -\frac{1}{nE} \hat{S}_{n,E}(z) \quad (\text{for sufficiently large } n, E) \\ &\xrightarrow{P} z^* \quad \text{as } n, E \rightarrow \infty. \end{aligned}$$

Next, we prove the posterior consistency at z^* .

By Assumption 3, $p(z^*) > 0$. Dividing both the numerator and denominator in the RHS of Eq. 12 by $p(z^*) \exp\{-S_{n,E}(z^*)\}$, the posterior can be expressed as

$$\hat{p}(z^* | \mathcal{D}) = \frac{1}{1 + \sum_{z \neq z^*} p(z)/p(z^*) \cdot \exp\{\hat{S}_{n,E}(z^*) - \hat{S}_{n,E}(z)\}}.$$

To show $\hat{p}(z^*|\mathcal{D}) \xrightarrow{P} 1$, it suffices to show that $\forall_p z \neq z^*$,

$$\exp\{\hat{S}_{n,E}(z^*) - \hat{S}_{n,E}(z)\} \xrightarrow{P} 0. \quad (15)$$

By Eq. 14, $\forall z \neq z^*$,

$$\frac{1}{nE} \left[\hat{S}_{n,E}(z^*) - \hat{S}_{n,E}(z) \right] \xrightarrow{P} \mu(z^*) - \mu(z) < 0.$$

Applying Lemma 2 to the above inequality, Eq. 15 holds. Hence we conclude the proof. ■

A.3 Proof of Theorem 2

Theorem (Posterior contraction rate) (Restatement of Theorem 2). *Given Assumptions 1 to 5, there exists a sequence $\epsilon_{n,E} = O(R \cdot e^{-\kappa n E \mu_{\min}})$ such that*

$$P\left(TV(\hat{p}(z | \mathcal{D}), \delta_{z^*}(z)) > \epsilon_{n,E}\right) \rightarrow 0$$

as $n \rightarrow \infty$ and $E \rightarrow \infty$, where

$$R = \left(\max_{z \neq z^*} \frac{p(z)}{p(z^*)} \right) \cdot |supp(p(z))|, \quad (16)$$

$$\mu(z) := \mathbb{E}_{p(e)p_e(x^z)} [\text{KL}[p_e(y | x^z) \| g(y | x^z)]], \quad (17)$$

$$\mu_{\min} := \min_{z \neq z^*, z \in supp(p(z))} \bar{\mu}(z), \quad (18)$$

and κ is a fixed value in $(0, 1)$.

Proof Based on the expression of the posterior in Eq. 12, we have the following lower bound on the posterior value at z^*

$$\hat{p}(z^* | \mathcal{D}) \geq \frac{1}{1 + R_{\max} \sum_{z \neq z^*} \exp\{\hat{S}_{n,E}(z^*) - \hat{S}_{n,E}(z)\}}. \quad (19)$$

where $R_{\max} := \max_{z \neq z^*} \frac{p(z)}{p(z^*)}$.

We decompose $\hat{S}_{n,E}(z)$ as follows:

$$\hat{S}_{n,E}(z) = S_{n,E}(z) + B_{n,E}(z) \quad (20)$$

where

$$S_{n,E}(z) := \sum_{e=1}^E \sum_{i=1}^{n_e} \log p_e(y_{ei} \mid x_{ei}^z) - \log g(y_{ei} \mid x_{ei}^z), \quad (21)$$

is the log-likelihood ratio under the true model, and

$$B_{n,E}(z) := \hat{S}_{n,E}(z) - S_{n,E}(z)$$

is the estimation bias of the log-likelihood ratios.

Step 1. We first show the concentration behavior of $S_{n,E}(z^*) - S_{n,E}(z)$.

For any $z \neq z^*$ and any $k > 0$, by Chebyshev's inequality we have

$$P\left(|S_{n,E}(z^*) - S_{n,E}(z) - \mathbb{E}[S_{n,E}(z^*) - S_{n,E}(z)]| \geq k \right) \leq \frac{\text{Var}[S_{n,E}(z^*) - S_{n,E}(z)]}{k^2}. \quad (22)$$

Note that by definitions of $\mu(z)$ and $v(z)$,

$$\mathbb{E}[S_{n,E}(z)] = nE\mu(z), \quad \text{Var}[S_{n,E}(z)] = nEv(z).$$

Furthermore we have

$$\mathbb{E}[S_{n,E}(z^*) - S_{n,E}(z)] = \mu(z^*) - \mu(z) < 0 \quad (23)$$

by Assumption 2, and

$$\text{Var} [S_{n,E}(z^*) - S_{n,E}(z)] \leq 2nEv_{\max} \quad (24)$$

where $v_{\max} := \max_z v(z) < \infty$ by Assumption 5.

Setting $k = (1 - \kappa)nE\mu(z)$ for a fixed value $\kappa \in (0, 1)$, and substituting the expressions for the mean and variance from Eq. 23 and Eq. 24 into Eq. 22, we obtain

$$P\left(|S_{n,E}(z^*) - S_{n,E}(z) + nE\mu(z)| \geq (1 - \kappa)nE\mu(z) \right) \leq \frac{2v_{\max}}{nE(1 - \kappa)^2\mu(z)^2}. \quad (25)$$

Step 2. We then show the concentration behavior of $B_{n,E}(z^*) - B_{n,E}(z)$.

By Assumption 4 and LLN, as $n \rightarrow \infty$ and $E \rightarrow \infty$, each estimation bias $\hat{B}_{n,E}(z)$ goes to 0, and so

$$\frac{1}{nE} [B_{n,E}(z^*) - B_{n,E}(z)] \xrightarrow{P} 0. \quad (26)$$

Step 3. Having characterized the concentration behaviors of $S_{n,E}(z)$ and $B_{n,E}(z)$, we are now ready to prove the posterior contraction rate.

We define the rate $\epsilon_{n,E}$ as follows

$$\epsilon_{n,E} := 1 - \frac{1}{1 + Re^{-\kappa nE\mu_{\min}}} = O(R \cdot e^{-\kappa nE\mu_{\min}}).$$

Our goal is to show

$$P\left(\text{TV}\left(p(z \mid \mathcal{D}), \delta_{z^*}(z)\right) > \epsilon_{n,E}\right) \rightarrow 0, \quad \text{as } n \rightarrow \infty \text{ and } E \rightarrow \infty.$$

Recall $\text{TV}\left(p(z \mid \mathcal{D}), \delta_{z^*}(z)\right) = 1 - p(z^* \mid \mathcal{D})$, it suffices to show that

$$P\left(\hat{p}\left(z^* \mid \mathcal{D}\right) < 1 - \epsilon_{n,E}\right) \xrightarrow{P} 0, \quad \text{as } n \rightarrow \infty \text{ and } E \rightarrow \infty.$$

Using the inequality that lower bounds $p(z^* \mid \mathcal{D})$ from Eq. 19, we have

$$\begin{aligned} & P\left(\hat{p}\left(z^* \mid \mathcal{D}\right) < 1 - \epsilon_{n,E}\right) \\ & \leq P\left(\frac{1}{1 + R_{\max} \sum_{z \neq z^*} \exp\{\hat{S}_{n,E}(z^*) - \hat{S}_{n,E}(z)\}} < 1 - \epsilon_{n,E}\right) \\ & = P\left(\frac{1}{1 + R_{\max} \sum_{z \neq z^*} \exp\{S_{n,E}(z^*) - S_{n,E}(z)\}} < 1 - \epsilon_{n,E} \mid \mathcal{A}_{n,E}^c\right) P(\mathcal{A}_{n,E}^c) \\ & \quad + P\left(\frac{1}{1 + R_{\max} \sum_{z \neq z^*} \exp\{S_{n,E}(z^*) - S_{n,E}(z)\}} < 1 - \epsilon_{n,E} \mid \mathcal{A}_{n,E}\right) P(\mathcal{A}_{n,E}) \end{aligned} \tag{27}$$

where $\mathcal{A}_{n,E}$ is the event that $\exists z \neq z^*$ such that $|S_{n,E}(z^*) - S_{n,E}(z) + nE\mu(z)| \geq \frac{1}{2}(1 - \kappa)nE\mu(z)$ or $|B_{n,E}(z^*) - B_{n,E}(z)| \geq \frac{1}{2}(1 - \kappa)nE\mu(z)$, and $\mathcal{A}_{n,E}^c$ denotes the complement of $\mathcal{A}_{n,E}$.

We consider the following two cases:

- (a) Given the event $\mathcal{A}_{n,E}$, by definition of $\mathcal{A}_{n,E}$ and the subadditivity of probability measure, we have

$$\begin{aligned} P(\mathcal{A}_{n,E}) & \leq \sum_{z \neq z^*} \left\{ P\left(|S_{n,E}(z^*) - S_{n,E}(z) + nE\mu(z)| \geq \frac{1}{2}(1 - \kappa)nE\mu(z)\right) \right. \\ & \quad \left. + P\left(|B_{n,E}(z^*) - B_{n,E}(z)| \geq \frac{1}{2}(1 - \kappa)nE\mu(z)\right) \right\}. \end{aligned}$$

As $n \rightarrow \infty$ and $E \rightarrow \infty$, the first term in the summation on the RHS of the inequality converges to zero by Eq. 25 from Step 1, and the term converges to

0 as well by Eq. 26 from Step 2. Thus,

$$P(\mathcal{A}_{n,E}) \rightarrow 0, \quad \text{as } n \rightarrow \infty \text{ and } E \rightarrow \infty. \quad (28)$$

(b) Given the complement event $\mathcal{A}_{n,E}^c$, $\forall z \neq z^*$ both $|S_{n,E}(z^*) - S_{n,E}(z) + nE\mu(z)| < \frac{1}{2}(1 - \kappa)nE\mu(z)$, and $|B_{n,E}(z^*) - B_{n,E}(z)| < \frac{1}{2}(1 - \kappa)nE\mu(z)$. By the triangle inequality and the decomposition of $\hat{S}_{n,E}(z)$ in Eq. 20, we have

$$\begin{aligned} & |\hat{S}_{n,E}(z^*) - \hat{S}_{n,E}(z^*) + nE\mu(z)| \\ &= |S_{n,E}(z^*) - S_{n,E}(z) + nE\mu(z) + B_{n,E}(z^*) - B_{n,E}(z)| < (1 - \kappa)nE\mu(z). \end{aligned}$$

Hence, $\mathcal{A}_{n,E}^c$ implies that

$$\hat{S}_{n,E}(z^*) - \hat{S}_{n,E} < -\kappa nE\mu(z), \quad \forall z \neq z^*$$

which further implies

$$\begin{aligned} \frac{1}{1 + R_{\max} \sum_{z \neq z^*} \exp\{S_{n,E}(z^*) - S_{n,E}(z)\}} &> \frac{1}{1 + R_{\max} \sum_{z \neq z^*} \exp\{-\kappa nE\mu(z)\}} \\ &> \frac{1}{1 + R \exp\{-\kappa nE\mu_{\min}\}} = 1 - \epsilon_{n,E} \end{aligned}$$

where the last inequality follows from the definitions of R and μ_{\min} in Eq. 16 and Eq. 18, respectively.

Therefore,

$$P\left(\frac{1}{1 + R_{\max} \sum_{z \neq z^*} \exp\{S_{n,E}(z^*) - S_{n,E}(z)\}} < 1 - \epsilon_{n,E} \mid \mathcal{A}_{n,E}^c\right) = 0. \quad (29)$$

Combining the analysis in these two cases, namely Eq. 28 and Eq. 29, with Eq. 27

we prove the final contraction rate result: as $n \rightarrow \infty$ and $E \rightarrow \infty$,

$$P\left(\hat{p}\left(z^* \mid \mathcal{D}\right) < 1 - \epsilon_{n,E}\right) \rightarrow 0.$$

■

A.4 Theory extensions to finite n and finite E cases

We present extensions of Theorems 1 and 2 to two separate cases: (1) E is held fixed while letting $n \rightarrow \infty$, and (2) n is held fixed while letting $E \rightarrow \infty$. These results corroborate the first part of § 3.2.

Case 1: E fixed and $n \rightarrow \infty$. Given fixed E environments $\mathcal{E}_{obs} = \{1, \dots, E\}$, we set the collection of environments of interests \mathcal{E} to \mathcal{E}_{obs} . Importantly, the pooled conditional $g(y \mid x^z)$ in Definition 1 and Assumption 1, which depend on \mathcal{E} , should adapt to \mathcal{E}_{obs} accordingly. We also re-define $p(e) = \frac{1}{E} \sum_{e'=1}^E \delta_{e'}(e)$ as a uniform distribution over the finite set \mathcal{E}_{obs} , and any expectation with respect to $p(e)$ should be re-interpreted.

We then make the following assumption:

Assumption 6 (Estimation consistency given fixed environments). *Given fixed E environments \mathcal{E}_{obs} , $\forall_p z$, as $n \rightarrow \infty$,*

$$\begin{aligned} \frac{1}{nE} \sum_{i=1}^n \sum_{e=1}^E \log \hat{p}_e(y_{ei} \mid x_{ei}^z) &\xrightarrow{P} \mathbb{E}_{p(e)p_e(y \mid x^z)} [\log p_e(y \mid x^z)], \\ \frac{1}{nE} \sum_{i=1}^n \sum_{e=1}^E \log \hat{g}(y_{ei} \mid x_{ei}^z) &\xrightarrow{P} \mathbb{E}_{g(y \mid x^z)} [\log g(y \mid x^z)]. \end{aligned}$$

Theorem 3 (Posterior consistency given infinite per-environment samples). *Given fixed E environments \mathcal{E} , and Assumptions 1 to 3 and 6, as $n \rightarrow \infty$, we have*

- *posterior mode consistency, i.e. $\hat{z}_{n,E} := \arg \max_z \hat{p}(z \mid \mathcal{D}) \xrightarrow{P} z^*$, and*
- *posterior consistency at z^* , i.e. $\hat{p}(z^* \mid \mathcal{D}) \xrightarrow{P} 1$.*

Theorem 4 (Posterior contraction rate given infinite per-environment samples). *Given Assumptions 1 to 3, 6 and 5, there exists a sequence $\epsilon_{n,E} = O(R \cdot e^{-\kappa n E \mu_{\min}})$ such that*

$$P\left(TV(p(z | \mathcal{D}), \delta_{z^*}(z)) > \epsilon_{n,E}\right) \rightarrow 0$$

as $n \rightarrow \infty$, where R and μ_{\min} are defined in Eq. 8 and Eq. 10, respectively, and κ is a fixed value in $(0, 1)$.

Assumption 4 is a modification of Assumption 4 where we only require the estimation consistency with respect to n within E environments.

The proofs of Theorems 3 and 4 are essentially the same as the proofs of Theorems 1 and 2, respectively, except that E is now held fixed, only taking $n \rightarrow \infty$. Hence we abbreviate them here.

Case 2: n fixed and $E \rightarrow \infty$. In this case, we consider a similar setting as in the main theorems where E environments are sampled from $p(e)$ – a uniform distribution over \mathcal{E} . Given the drawn E environments, we relabel them by $e = 1, \dots, E$. And in each environment e , we draw n observations x_{ei}, y_{ei} i.i.d. from $p_e(x, y)$ for $i = 1, \dots, n$.

Assumption 7 (Estimation consistency of pooled conditional given fixed n). *Given fixed n , $\forall_p z$, as $E \rightarrow \infty$,*

$$\frac{1}{n} \frac{1}{E} \sum_{i=1}^n \sum_{e=1}^E \log \hat{g}(y_{ei} | x_{ei}^z) \xrightarrow{P} \mathbb{E}_{p(e)p_e(x^z, y)} [\log g(y | x^z)].$$

Assumption 8 (Identifiability of z^* under estimation bias). *z^* minimizes $\mu_n(z)$ defined as follows*

$$\begin{aligned} \mu_n(z) := & \underbrace{\mathbb{E}_{p(e)p_e(x^z)} \text{KL}[p_e(y | x^z) \| g(y | x^z)]}_{:= \text{model discrepancy } \mu(z)} \\ & + \underbrace{\frac{1}{n} \mathbb{E}_{p(e) \prod_{i=1}^n p_e(x_i, y_i)} \sum_{i=1}^n [\log \hat{p}_e^z(y_i; x_i^z) - \log p_e(y_i | x_i^z)]}_{:= \text{estimation bias of per-environment conditionals } b_n(z)}, \end{aligned} \tag{30}$$

Theorem 5 (Posterior consistency given infinite environments). *Given fixed n and Assumptions 1 to 3, 7 and 8, as $E \rightarrow \infty$, we have*

1. *posterior mode consistency, i.e. $\hat{z}_{n,E} \xrightarrow{P} z^*$*
2. *posterior consistency at z^* , i.e. $\hat{p}(z^* | \mathcal{D}) \xrightarrow{P} 1$.*

Assumption 7 ensures that the pooled model is consistently estimated given infinite environments, given finite data in each environments. This assumption is reasonable, as we view each observation (x_{ei}, y_{ei}) as i.i.d. copy from the pooled distribution $g(x, y) := \int p(e)p_e(x, y)de$.

Assumption 8 is a *non-trivial* assumption – it requires that the invariant z^* minimizes the combined value of model discrepancy $\mu(z)$ and local model estimation bias $b_n(z)$. Since z^* minimizes $\mu(z)$ by Assumption 2, Assumption 8 is satisfied whenever the estimation bias is well-controlled, for example, if $\max_z |b_n(z)| < \min_{z: z \neq z^*} \mu(z)$. In practice, when the per-environment sample size n is sufficiently large, the estimation bias becomes negligible, so that Assumption 8 is expected to hold.

Incorporating these two assumptions, Theorem 5 establishes posterior consistency in the infinite environment regime. The proof follows the same structure as the proof of Theorem 1.

Proof $\forall z$, by law of large number (LLN), as $E \rightarrow \infty$

$$\begin{aligned} \frac{1}{nE} \sum_{i=1}^n \sum_{e=1}^E [\log \hat{p}_e(y_{ei} | x_{ei}^z) - \log p_e(y_{ei} | x_{ei}^z)] &\xrightarrow{P} b_n(z), \\ \frac{1}{nE} \sum_{i=1}^n \sum_{e=1}^E \log g(y | x^z) &\xrightarrow{P} \mathbb{E}_{p(e)p_e(x^z, y)} [\log g(y | x^z)], \\ \frac{1}{nE} \sum_{i=1}^n \sum_{e=1}^E \log p_e(y | x^z) &\xrightarrow{P} \mathbb{E}_{p(e)p_e(x^z, y)} [\log p_e(y | x^z)]. \end{aligned} \quad (31)$$

By Assumption 7 and Eq. 31, and recall the definitions of $\mu(z)$ in Eq. 9 and $\hat{S}_{n,E}(z)$ in Eq. 13, we have $\forall_p z$,

$$\frac{1}{nE} \hat{S}_{n,E}(z) \xrightarrow{P} \mu_n(z) \quad (32)$$

Applying Lemma 1, as $E \rightarrow \infty$

$$\arg \max_{z:p(z)>0} -\frac{1}{nE} \hat{S}_{n,E}(z) \xrightarrow{P} \arg \max_{z:p(z)>0} -\mu_n(z) = z^*,$$

where the last equality follows from Assumption 8.

Using the posterior expression in Eq. 12, we show that the posterior mode is consistent:

$$\begin{aligned} \hat{z}_{n,E} &:= \arg \max_z \hat{p}(z \mid \mathcal{D}) \\ &= \arg \max_{z:p(z)>0} \log p(z) - \hat{S}_{n,E}(z) \\ &= \arg \max_{z:p(z)>0} \frac{1}{nE} \log p(z) - \frac{1}{nE} \hat{S}_{n,E}(z) \\ &= \arg \max_{z:p(z)>0} -\frac{1}{nE} \hat{S}_{n,E}(z) \\ &\xrightarrow{P} z^*. \end{aligned}$$

Next, we prove the posterior consistency at z^* .

By Assumption 3, $p(z^*) > 0$. Dividing both the numerator and denominator in the RHS of the posterior expression in Eq. 12 by $p(z^*) \exp\{-S_{n,E}(z^*)\}$, the posterior reduces to

$$\hat{p}(z^* \mid \mathcal{D}) = \frac{1}{1 + \sum_{z \neq z^*} p(z)/p(z^*) \cdot \exp\{\hat{S}_{n,E}(z^*) - \hat{S}_{n,E}(z)\}}. \quad (33)$$

To show $\hat{p}(z^* \mid \mathcal{D}) \xrightarrow{P} 1$ as $E \rightarrow \infty$, it suffices to show that $\forall_p z \neq z^*$,

$$\exp\{\hat{S}_{n,E}(z^*) - \hat{S}_{n,E}(z)\} \xrightarrow{P} 0. \quad (34)$$

By Eq. 32, $\forall z \neq z^*$, as $E \rightarrow \infty$,

$$\frac{1}{nE} \left[\hat{S}_{n,E}(z^*) - \hat{S}_{n,E}(z) \right] \xrightarrow{P} \mu_n(z^*) - \mu_n(z) < 0.$$

Applying Lemma 2 to the above inequality, Eq. 34 holds. Hence we conclude the proof. ■

Next we establish the contraction rate result. Since the local model estimation bias is non-negligible, we need an additional assumption on its variance:

Assumption 9 (Finite variance of estimation bias in per-environment models). *For any fixed n , the variance of the estimation bias of per-environment conditionals*

$$v_n(z) := \text{Var}_{p(e) \prod_{i=1}^n p_e(y_i | x_i^z)} \left[\sum_{i=1}^n (\log \hat{p}_e(y_i | x_i^z) - \log p_e(y_i | x_i^z)) \right]$$

exists and is finite.

Theorem 6 (Contraction rate given infinite environments). *Given Assumptions 1 to 3, 7, 8, 5 and 9, for any fixed n , there exists a sequence $\epsilon_{n,E} = O(Re^{-\kappa n E \mu_{\min}})$ such that*

$$P\left(TV(p(z | \mathcal{D}), \delta_{z^*}(z)) > \epsilon_{n,E}\right) \rightarrow 0 \quad (35)$$

as $E \rightarrow \infty$, where R and μ_{\min} are defined in Eq. 8 and Eq. 10, respectively, and κ is a fixed value in $(0, 1)$.

Proof We consider the same posterior lower bound in Eq. 19, and decompose $\hat{S}_{n,E}(z)$ as follows

$$\hat{S}_{n,E}(z) = S_{n,E}(z) + B_{n,E}^{(1)}(z) - B_{n,E}^{(2)}(z),$$

where $S_{n,E}(z)$ is the log-likelihood ratio under the true model in Eq. 21, and

$$\begin{aligned} B_{n,E}^{(1)}(z) &= \sum_{i=1}^n \sum_{e=1}^E \log \hat{p}_e(y_{ei} | x_{ei}^z) - \log p_e(y_{ei} | x_{ei}^z) \\ B_{n,E}^{(2)}(z) &= \sum_{i=1}^n \sum_{e=1}^E \log \hat{g}(y_{ei} | x_{ei}^z) - \log g(y_{ei} | x_{ei}^z) \end{aligned}$$

are the estimation biases of log-likelihood ratios of local and pooled models, respectively.

We follow a similar 3-step proof strategy as in the proof of Theorem 2.

Step 1. We first show the concentration behavior of $d_{n,E}(z^*, z) := S_{n,E}(z^*) + B_{n,E}^{(1)}(z^*) - S_{n,E}(z) - B_{n,E}^{(1)}(z)$ with respect to E .

For any fixed $\kappa \in (0, 1)$, by Chebyshev's inequality, $\forall z \neq z^*$,

$$P\left(\left|d_{n,E}(z^*, z) - \mathbb{E}[d_{n,E}(z^*, z)]\right| \geq \frac{1-\kappa}{2} \left|\mathbb{E}[d_{n,E}(z^*, z)]\right|\right) \leq \frac{\text{Var}[d_{n,E}(z^*, z)]}{(1-\kappa)^2/4 \cdot \mathbb{E}[d_{n,E}(z^*, z)]^2}. \quad (36)$$

Note that

$$\mathbb{E}[d_{n,E}(z^*, z)] = -nE\mu_n(z, z^*) \quad (37)$$

where $\mu_n(z, z^*) := \mu_n(z) - \mu_n(z^*) > 0$ by Assumption 8, and

$$\text{Var}[d_{n,E}(z^*, z)] \leq 2nEv_{n,\max}, \quad (38)$$

where $v_{n,\max} := \max_z v_n(z) + \max_z v(z)$ is finite given Assumptions 5 and 9.

Substituting Eq. 37 and Eq. 38 into Eq. 36, we have

$$P\left(\left|d_{n,E}(z^*, z) + nE\mu_n(z, z^*)\right| \geq \frac{1-\kappa}{2} nE\mu_n(z, z^*)\right) \leq \frac{2v_{n,\max}}{nE(1-\kappa)^2/4\mu_n(z, z^*)^2}. \quad (39)$$

Step 2. We then show the concentration behavior of $B_{n,E}^{(2)}(z^*) - B_{n,E(z)}^{(2)}$ with respect to E .

By Assumption 7 and LLN, $\forall z$, as $E \rightarrow \infty$,

$$\frac{1}{nE} B_{n,E}^{(2)}(z^*) - B_{n,E}^{(2)}(z) \xrightarrow{P} 0. \quad (40)$$

Step 3. Having characterized the above concentration behaviors, we now prove the contrac-

tion rate defined as

$$\epsilon_{n,E} := 1 - \frac{1}{1 + Re^{-\kappa n E \mu_{\min}}} = O(R \cdot e^{-\kappa n E \mu_{\min}}).$$

We define $\mathcal{A}_{n,E}$ be the event that $\exists z \neq z^*$ such that $|d_{n,E}(z^*, z) + nE\mu_n(z, z^*)| \geq \frac{1-\kappa}{2}nE\mu_n(z, z^*)$, or $|B_{n,E}^{(2)}(z^*) - B_{n,E}^{(2)}(z)| \geq \frac{1-\kappa}{2}nE\mu_n(z, z^*)$.

Following a similar analysis in the proof of Theorem 2, we can show that as $E \rightarrow \infty$

$$P\left(\text{TV}(\hat{p}(z | \mathcal{D}), \delta_{z^*}(z)) > \epsilon_{n,E}\right) = P\left(\hat{p}(z^* | \mathcal{D}) < 1 - \epsilon_{n,E}\right) \leq P(\mathcal{A}_{n,E}) \rightarrow 0$$

where the last convergence follows from Eq. 39 and Eq. 40. ■

A.5 Theory generalization under relaxed assumptions

We provide a generalization of Theorem 1 under more general conditions. This result supports the discussion in § 3.2 where some of the original assumptions are violated.

We define the best-fitting local model $\bar{p}_e(y | x^z)$ and pooled model $\bar{g}(y | x^z)$ within the chosen model class $\mathcal{P}_{y|x^z}$:

$$\begin{aligned} \bar{p}_e(y | x^z) &:= \arg \max_{\tilde{p}(y|x^z) \in \mathcal{P}_{y|x^z}} \mathbb{E}_{p_e(x,y)} \log \tilde{p}(y | x^z), \quad \forall e, z \\ \bar{g}(y | x^z) &:= \arg \max_{\tilde{p}(y|x^z) \in \mathcal{P}_{y|x^z}} \sum_{e \in \mathcal{E}} \mathbb{E}_{p_e(x,y)} \log \tilde{p}(y_{ei} | x_{ei}^z), \quad \forall z, \end{aligned}$$

and the expected discrepancy between them

$$\bar{\mu}(z) := \mathbb{E}_{p(e)p_e(x,y)} [\log \bar{p}_e(y | x^z) - \log \bar{g}(y | x^z)]. \quad (41)$$

Theorem 7 (Posterior consistency under general conditions). *Let $\bar{\mathcal{Z}}^*$ be the set of minimizer(s) of $\bar{\mu}(z)$ defined in Eq. 41. Assume that $p(\bar{\mathcal{Z}}^*) > 0$, and $\forall_p z$, as $n \rightarrow \infty$ and*

$E \rightarrow \infty$,

$$\begin{aligned} & \frac{1}{nE} \sum_{i=1}^n \sum_{e=1}^E \log \hat{p}_e(y_{ei} \mid x_{ei}^z) \xrightarrow{P} \mathbb{E}_{p(e)p_e(y,x^z)} [\log \bar{p}_e(y \mid x^z)], \\ \text{and } & \frac{1}{nE} \sum_{i=1}^n \sum_{e=1}^E \log \hat{g}(y_{ei} \mid x_{ei}^z) \xrightarrow{P} \mathbb{E}_{p(e)p_e(y,x^z)} [\log \bar{g}(y \mid x^z)]. \end{aligned} \tag{42}$$

Then as $n \rightarrow \infty$ and $E \rightarrow \infty$, we have

- $P(\hat{z}_{n,E} \in \bar{\mathcal{Z}}^*) \rightarrow 1$,
- $\hat{p}(\bar{\mathcal{Z}}^* \mid \mathcal{D}) \xrightarrow{P} 1$.

Theorem 7 extends the posterior consistency result in Theorem 1 to a more general setting. The positive prior condition is now imposed on the set of minimizers $\bar{\mathcal{Z}}^*$ of the discrepancy measure between the best-fitting local and pooled models. Similarly, the estimation consistency condition in Eq. 42 is adapted to these models as well. As a result, the posterior concentrates on $\bar{\mathcal{Z}}^*$, which can be interpreted as the most *approximately* invariant feature selectors.

Theorem 1 can be viewed as a special instance of Theorem 7 under stricter assumptions: the model is correctly specified, and the exact invariant feature selector z^* exists, is unique and has positive prior mass. The proof follows a similar structure as that of Theorem 1.

Proof We recall the posterior expression

$$\hat{p}(z \mid \mathcal{D}) = \frac{p(z) \exp\{-\hat{S}_{n,E}(z)\}}{\sum_z p(z) \exp\{-\hat{S}_{n,E}(z)\}}$$

where $\hat{S}_{n,E}(z)$ is the log-likelihood ratio given z ,

$$\hat{S}_{n,E}(z) := \sum_{i=1}^n \sum_{e=1}^E \log \hat{p}_e(y_{ei} \mid x_{ei}^z) - \log \hat{g}(y_{ei} \mid x_{ei}^z).$$

By our assumption, as $n, E \rightarrow \infty$,

$$\frac{1}{nE} \hat{S}_{n,E}(z) \xrightarrow{P} \mathbb{E}_{p(e)p_e(y|x^z)} [\log \bar{p}_e(y | x^z)] - \mathbb{E}_{p(e)p_e(y|x^z)} [\log \bar{g}(y | x^z)] = \bar{\mu}(z). \quad (43)$$

For large nE , we have

$$\begin{aligned} \hat{z}_{n,E} &:= \arg \max_z \hat{p}(z | \mathcal{D}) \\ &= \arg \max_{z:p(z)>0} \log p(z) - \hat{S}_{n,E}(z) \\ &= \arg \max_{z:p(z)>0} -\frac{1}{nE} \hat{S}_{n,E}(z). \end{aligned}$$

By Lemma 1 and Eq. 43, as $n \rightarrow \infty$ and $E \rightarrow \infty$

$$P(\hat{z}_{n,E} \in \bar{\mathcal{Z}}^*) \rightarrow 1.$$

where we recall $\bar{\mathcal{Z}}^*$ is the set of minimizers of $\bar{\mu}(z)$.

Next, we consider any $z \notin \bar{\mathcal{Z}}^*$ with $p(z) > 0$. Then

$$\begin{aligned} \hat{p}(z | \mathcal{D}) &\leq \frac{p(z) \exp\{-\hat{S}_{n,E}(z)\}}{p(z) \exp\{-\hat{S}_{n,E}(z)\} + \sum_{z' \in \bar{\mathcal{Z}}^*} p(z') \exp\{-\hat{S}_{n,E}(z')\}} \\ &= \frac{1}{1 + \sum_{z' \in \bar{\mathcal{Z}}^*} p(z')/p(z) \exp\{\hat{S}_{n,E}(z) - \hat{S}_{n,E}(z')\}}. \end{aligned}$$

Note that by our assumption, $\forall z' \in \bar{\mathcal{Z}}^*$,

$$\frac{1}{nE} \left(\hat{S}_{n,E}(z) - \hat{S}_{n,E}(z') \right) \xrightarrow{P} \bar{\mu}(z) - \bar{\mu}(z') > 0,$$

and consequently by Lemma 2, we have $\exp\{\hat{S}_{n,E}(z) - \hat{S}_{n,E}(z')\} \xrightarrow{P} \infty$.

Consequently, $\forall z \notin \bar{\mathcal{Z}}^*$, $\hat{p}(z | \mathcal{D}) \xrightarrow{P} 0$, and therefore $\hat{p}(\bar{\mathcal{Z}}^* | \mathcal{D}) \xrightarrow{P} 1$. ■

Algorithm 3: U2G gradient estimation [Yin et al., 2020]

Input: Objective function f , dataset \mathcal{D} , variational parameter ϕ

Output: A random unbiased estimate \hat{g} of $\nabla_{\phi} \mathbb{E}_{q_{\phi}(z)} [f(z, \mathcal{D}, \phi)]$

- 1 Draw $u \sim \prod_{i=1}^p \text{Uniform}[0, 1]$
 - 2 $z_1 \leftarrow \mathbf{1}[u > 1 - \text{sigmoid}(\phi)], z_2 \leftarrow \mathbf{1}[u < \text{sigmoid}(\phi)]$
 - 3 $\hat{g} \leftarrow \frac{1}{2} \text{sigmoid}(|\phi|) \cdot [f(z_1, \mathcal{D}, \phi) - f(z_2, \mathcal{D}, \phi)] \cdot (z_1 - z_2)$
-

B Details on VI-BIP

We provide additional details on VI-BIP, including gradient estimation, optimization guidelines and implementation considerations.

B.1 Gradient estimators for binary latent variables

Optimizing VI-BIP requires computing gradients of the ELBO in Eq. 7, which involves expectations with respect to the discrete variational distribution $q_{\phi}(z)$. To obtain an unbiased gradient estimate, we use the U2G estimator proposed by Yin et al. [2020].

Algorithm 3 describes the general U2G estimator for computing an unbiased estimate of $\nabla_{\phi} \mathbb{E}_{q_{\phi}(z)} [f(z, \mathcal{D}, \phi)]$, given an objective function f , dataset \mathcal{D} , and variational parameters ϕ . The algorithm constructs a single gradient estimate using pair of correlated samples z_1 and z_2 to reduce variance while maintaining unbiasedness. Multiple gradient estimates can be obtained by independently repeating this procedure, and their average is used to form the final gradient estimate.

To use U2G in our setting (Algorithm 2), the objective function corresponds to the integrand inside the ELBO expression from Eq. 7, that is,

$$f(z, \mathcal{D}, \phi) := [\log p(z) + \sum_{e=1}^E \sum_{i=1}^{n_e} \log \frac{\hat{g}(y_{ei} | x_{ei}^z)}{\hat{p}_e(y_{ei} | x_{ei}^z)} - \log q_{\phi}(z)], \quad (44)$$

where we replace the true pooled and local conditionals in the ELBO with estimated counterparts.

B.2 Optimization guidelines

We provide guidelines for setting and tuning the hyperparameters. All of these hyperparameters can be tuned by monitoring the training-set ELBO and the overall optimization behavior. In general, we expect a gradually increasing ELBO trend during training, with higher ELBO values indicating better model fit. We refer to experiment sections for exact configurations used in each setting.

The key hyperparameters are as follows:

- Number of stochastic gradient samples M : At each iteration, we estimate the gradient of the ELBO using M samples. Increasing M can reduce the variance but increase the computational cost. In our experiments, we found that using M between 10 and 20 strikes a good balance between performance and computational cost.
- Prior $p(z)$: The choice of prior is crucial in high-dimensional settings, as it influences the sparsity of the inferred invariant sets and the initialization of variational parameters (see below). We recommend restricting the prior support to feature subset at size at most p_{\max} , which can be informed by the domain knowledge. In practice, we found that the choice of p_{\max} can affect optimization dynamics and can be treated as a tunable hyperparameter.
- Initialization of variational parameters ϕ : The variational parameters ϕ are initialized to ensure that the expected number of invariant features is within the prior support. Specifically, we recommend initializing ϕ at ϕ_0 such that

$$\mathbb{E}_{q_{\phi_0}(z)} [\|z\|_0] \leq \max_{z:p(z)>0} \|z\|_0.$$

- Optimizer: We use stochastic gradient descent (SGD) throughout all experiments, following the practice of the original U2G paper [Yin et al., 2020].
- Learning rate scheduling: We use a cyclical learning rate scheduler [Smith, 2017] to

encourage mode exploration. However, alternative schedulers could be explored.

- Number of optimization steps: The number of optimization steps should be chosen based on the problem scale and convergence behavior. In our experiments, we set a fixed budget for the total number of optimization steps and select the iteration with the highest training-set ELBO.

B.3 Implementation details

We discuss several algorithmic techniques for Algorithm 2 that offer practical benefits.

- Analytical KL gradients: The ELBO in Eq. 7 can be decomposed into an expected likelihood term and a KL regularization term (up to a constant C)

$$\mathcal{L}(\mathcal{D}, \phi) = \mathbb{E}_{q_\phi(z)} \left[\sum_{e=1}^E \sum_{i=1}^{n_e} \log \frac{g(y_{ei} | x_{ei}^z)}{p_e(y_{ei} | x_{ei}^z)} \right] + \text{KL} [q_\phi(z) \| p(z)] + C,$$

Notably, under a uniform prior, the KL regularization term admits a closed-form gradient expression:

$$\nabla_\phi \text{KL} [q_\phi(z) \| p(z)] = [\log(\sigma) - \log(1 - \sigma)] \sigma(1 - \sigma) \Big|_{\sigma = \frac{1}{1+e^{-\phi}}}$$

To balance variance reduction with the implicit generalization behavior of stochastic gradients, we can consider a hybrid strategy: at each iteration, with some probability, we compute the analytical gradient of the KL term; otherwise, we use its stochastic estimate via the U2G estimator in Algorithm 3. The gradient of the reconstruction term, $\nabla_\phi \mathbb{E}_{q_\phi(z)} \left[\sum_{e=1}^E \sum_{i=1}^{n_e} \log \frac{g(y_{ei} | x_{ei}^z)}{p_e(y_{ei} | x_{ei}^z)} \right]$, is always estimated by U2G.

- Informative prior: In settings where the prior imposes a maximum number of invariant features p_{\max} or restricts the support with in other ways, we design a tractable optimization procedure that enforces these constraints.

Specifically, during each U2G estimation step, we draw a pair of correlated samples of z (Algorithm 3, Line 2). Since the variational distribution does not explicitly

encode prior constraints, it is possible for some sampled z to fall outside of the prior support, resulting in an infeasible objective value in Eq. 44, where $\log p(z) = -\infty$.

To address this issue, we manually assign a fixed, low objective value for infeasible z samples, to guide the optimization to toward high-objective regions within the feasible support. This penalty can be tuned for the specific task, typically by referencing the range of feasible objective values. In all of our experiments, we set this penalty value to -1 .

C Synthetic data study

We first describe the generic data generative process, and then we provide details for each experiment in Supplementary Sections C.1 to C.3.

1. **The factorization of the joint distribution.** To simulate multi-environment data, we specify a series of joint distributions that factorize consistently across environments:

$$p(x^{(1:p)}, y) = \prod_{i=1}^{p+1} p(t^{(i)} \mid t^{(1:i-1)}),$$

where permutation π is drawn uniformly over $[1, \dots, p+1]$, and $t^{(i)} = x^{(\pi(i))}$ if $\pi(i) \neq p+1$ and $t^{(i)} = y$ otherwise.¹ For convenience, we define $t^{(1:0)}$ to be an empty conditioning set.

Each conditional density is a linear Gaussian family, that is, $p(t^{(i)} \mid t^{(1:i-1)}) = \mathcal{N}(t^{(i)} \mid \beta t^{(1:i-1)} + \beta_0, \sigma^2)$ for some β, β_0, σ^2 .

We next specify the joint distributions corresponding to different environments.

2. **Observational environment $e = 1$.** For $i = 1, \dots, p+1$:

- sample the intercept parameter from $\mathcal{N}(0, 1)$,

¹If there are pre-specified lower bound p_{\min}^* and upper bound p_{\max}^* on the number of the true invariant features $\|z^*\|_0$, we keep uniformly sampling π until we get a π such that $p_{\min}^* < \pi^{-1}(p+1) \leq p_{\max}^* + 1$.

- sample the variance parameter from $\text{Uniform}([\sigma_{\min}^2, \sigma_{\max}^2])$, where σ_{\min}^2 and σ_{\max}^2 are lower and upper bounds on the variance parameter,
- sample each coefficient value independently:
 - if $\pi(i) = p+1$, i.e. $t^{(i)} = y$, first sample its absolute value from $\text{Uniform}([lb, ub])$ and then assign a random sign;
 - if $\pi(i) \neq p+1$ i.e. $t^{(i)} = x^{(\pi(i))}$, (i) with probability $actprob \in [0, 1]$ first sample its absolute value from $\text{Uniform}([lb, ub])$ and then assign a random sign, (ii) otherwise set to 0.

3. **Interventional Environments** ($e = 2, \dots, E$) Based on the observational environment $e = 1$, we first randomly draw a fraction $intfrac_e$ of features $x'_e \subset x$ to be intervened on. Then, for $i = 1, \dots, p+1$:

- If $t^{(i)} \notin x'_e$, set $p_e(t^{(i)} \mid t^{(1:i-1)}) = p_1(t^{(i)} \mid t^{(1:i-1)})$
- Otherwise, draw new parameters for $p_e(t^{(i)} \mid t^{(1:i-1)})$
 - sample intercept parameter by first sampling its absolute value from $\mathcal{N}(m_e, 1)$ and assigning to it a random sign, for some $m_e \in \mathbb{R}$ specific to the environment e .
 - sample variance parameter from $\text{Uniform}([\sigma_{e,\min}^2, \sigma_{e,\max}^2])$, where $\sigma_{e,\min}^2, \sigma_{e,\max}^2$ are the lower and upper bounds of variance parameters specific to the environment e .
 - sample each coefficient value independently:
 - * with probability $changeprob_e$, copy the corresponding coefficient from $e = 1$ case
 - * with probability $1 - changeprob_e$, (i) with probability $actprob$ sample its absolute value from $\text{Uniform}([lb_e, ub_e])$, assign a random sign and (ii) otherwise set to 0.

4. **Draw data.** Finally, we can draw n data points $\{x_{ei}, y_{ei}\}_{i=1}^n$ from each environment e independently, for $e = 1, \dots, E$.

C.1 Empirical verification of theory

We include simulation details for the experiments in § 4.1. We set $p = 3$, the maximum number of the true invariant features $p_{\max}^* = 3$, and the minimum number $p_{\min}^* = 1$. For $e = 1$, the lower bound of the absolute coefficient value $lb = 0.5$, upper bound $ub = 2$; $actprob = 1.0$; noise level lower bound $\sigma_{\min} = 0.1$ and upper bound $\sigma_{\max} = 0.2$. For $e = 2, \dots, E$,

C.2 Uncertainty quantification in limited environments

We provide the data generative process for the experiment in § 4.2, and include additional examples. All experiments are simulated with $n = 200$ per-environment samples.

Example 1. We provide the data generative process for the experiment in § 4.2. The joint distributions $\{p_e(x, y)\}_{e=1}^3$ factorize as follows

$$\begin{aligned} p_1(x, y) &= p_1(x^{(1)})p(y \mid x^{(1)})p_1(x^{(2)} \mid y) \\ p_2(x, y) &= p_2(x^{(1)})p(y \mid x^{(1)})p_3(x^{(2)} \mid y) \\ p_3(x, y) &= p_1(x^{(1)})p(y \mid x^{(1)})p_1(x^{(2)} \mid x^{(1)}, y) \end{aligned}$$

where

$$\begin{aligned} p_1(x^{(1)}) &= \mathcal{N}(x^{(1)} \mid 0, 0.1^2), \quad p_2(x^{(1)}) = \mathcal{N}(x^{(1)} \mid 2, 0.1^2), \quad p_3(x^{(1)}) = \mathcal{N}(x^{(1)} \mid 5, 0.1^2), \\ p(y \mid x^{(1)}) &= \mathcal{N}(y \mid x^{(1)} + 0.5, 0.1^2), \\ p_1(x^{(2)} \mid y) &= p_2(x^{(2)} \mid y) = \mathcal{N}(x^{(2)} \mid y + 0.1, 0.1^2), \\ p_3(x^{(2)} \mid x^{(1)}, y) &= \mathcal{N}(x^{(2)} \mid x^{(1)} + y + 0.1, 0.1^2). \end{aligned}$$

Considering only the first two environments $(p_1(x, y), p_2(x, y))$, both $x^{(1)}$ and $x^{(1:2)}$ are invariant features. As a result, the posterior places mass on both $z = [1, 0]$ and $z = [1, 1]$, as shown in Figure 2 (left). When the third environment $(p_3(x, y))$ is introduced, only $x^{(1)}$

remains invariant, and the posterior consequently concentrates on $z = [1, 0]$, as shown in Figure 2 (right).

In addition, we include the following two examples where there exist multiple invariant solutions in limited number of environments. In both cases, when $E = 2$, there are two sets of invariant features within the first two environments; but after we include a third environment, only one set of invariant features remains. We observe similar uncertainty quantification behaviors as in Example 1.

Example 2. The joint distributions $\{p_e(x, y)\}_{e=1}^3$ are given by

$$\begin{aligned} p_1(x, y) &= p_1(x^{(1)})p_1(x^{(2)})p(y \mid x^{(1)}, x^{(2)}) \\ p_2(x, y) &= p_2(x^{(1)})p_2(x^{(2)})p(y \mid x^{(1)}, x^{(2)}) \\ p_3(x, y) &= p_3(x^{(1)})p_3(x^{(2)})p(y \mid x^{(1)}, x^{(2)}) \end{aligned}$$

where

$$\begin{aligned} p_1(x^{(1)}) &= \mathcal{N}(x^{(1)} \mid 0, 0.1^2), \quad p_2(x^{(1)}) = \mathcal{N}(x^{(1)} \mid 2, 0.1^2), \quad p_3(x^{(1)}) = \mathcal{N}(x^{(1)} \mid 5, 0.1^2) \\ p_1(x^{(2)}) &= p_2(x^{(2)}) = \mathcal{N}(x^{(2)} \mid 0.5, 0.1^2), \quad p_3(x^{(2)}) = \mathcal{N}(x^{(2)} \mid -0.5, 0.1^2) \\ p(y \mid x^{(1)}, x^{(2)}) &= \mathcal{N}(y \mid x^{(1)} + x^{(2)} + 0.1, 0.1^2). \end{aligned}$$

$x^{(1:2)}$ is the only set of invariant features across $\mathcal{E} = \{1, 2, 3\}$ with $z^* = [1, 1]$ the invariant feature selector. But within the first two environments $\mathcal{E}' = \{1, 2\}$, $z = [1, 0]$ is also an invariant feature selector: By Definition 1, the pooled conditional within \mathcal{E}' is

$$\begin{aligned} g_{\mathcal{E}'}(y \mid x^{(1)}) &:= \frac{\sum_{e \in \mathcal{E}'} \int p(e)p_e(x, y) dx^{(2)}}{\sum_{e \in \mathcal{E}'} p(e)p_e(x^{(1)})} \\ &= \frac{\int \frac{1}{2}p_1(x^{(1)})p_1(x^{(2)})p(y \mid x^{(1)}, x^{(2)}) + \frac{1}{2}p_2(x^{(1)})p_2(x^{(2)})p(y \mid x^{(1)}, x^{(2)}) dx^{(2)}}{\frac{1}{2}p_1(x^{(1)}) + \frac{1}{2}p_2(x^{(1)})} \\ &= \int \frac{1}{2}p_1(x^{(2)})p(y \mid x^{(1)}, x^{(2)}) + \frac{1}{2}p_2(x^{(2)})p(y \mid x^{(1)}, x^{(2)}) dx^{(2)} \\ &= p_1(y \mid x^{(1)}) = p_2(y \mid x^{(1)}), \end{aligned}$$

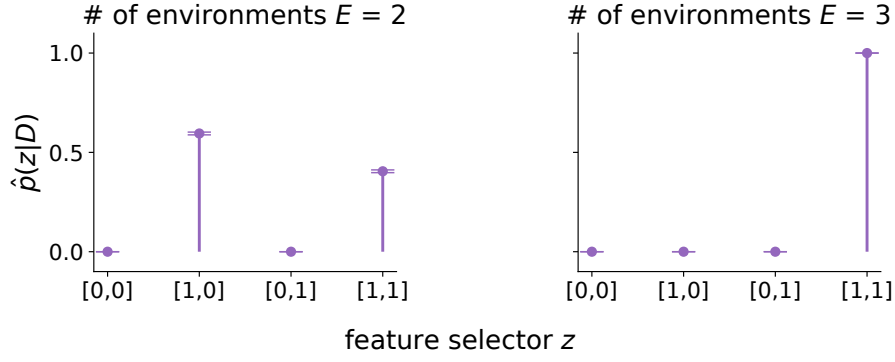


Figure S1: Synthetic study (Example 2): uncertainty quantification with $p = 2$ features. With $E = 2$ environments (left), the posterior $\hat{p}(z | \mathcal{D})$ is multi-modal over invariant selectors $z = [1, 0]$ and $[1, 1]$. For $E = 3$ (right), only $z = [1, 1]$ remains invariant, and the posterior concentrates at this solution. All results are averaged over 1,000 simulations with 95% confidence bands.

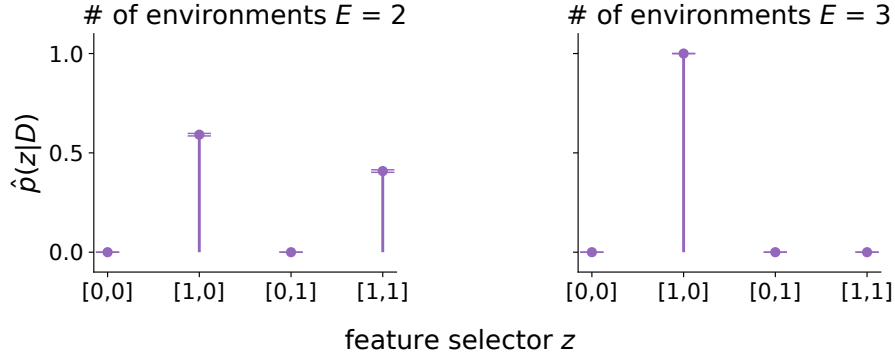


Figure S2: Synthetic study (Example 3): uncertainty quantification with $p = 2$ features. For $E = 2$ (left), the posterior $\hat{p}(z | \mathcal{D})$ is multi-modal over invariant selectors $[1, 0]$ and $[1, 1]$. With $E = 3$ (right), only $[1, 0]$ remains invariant, and the posterior concentrates at this value. All results are averaged over 1,000 simulations with 95% confidence bands.

where the last equality follows from $p_1(x^{(2)}) = p_2(x^{(2)})$. This result shows that $p_e(y | x^{(1)})$ is invariant within environments $\mathcal{E}' = \{1, 2\}$. However, one can show that it is not the case when we extend to $\mathcal{E} = \{1, 2, 3\}$, as $p_3(y | x^{(1)}) \neq p_1(y | x^{(1)})$. The corresponding posterior distributions for the two scenarios are shown in Figure S1.

Example 3. The joint distributions $\{p_e(x, y)\}_{e=1}^3$ are given by

$$p_1(x, y) = p_1(x^{(1)})p(y | x^{(1)})p_1(x^{(2)} | x^{(1)})$$

$$p_2(x, y) = p_2(x^{(1)})p(y | x^{(1)})p_2(x^{(2)} | x^{(1)})$$

$$p_3(x, y) = p_3(x^{(1)})p(y | x^{(1)})p_3(x^{(2)} | x^{(1)}, y)$$

where

$$\begin{aligned}
p_1(x^{(1)}) &= \mathcal{N}(x^{(1)} \mid 0, 0.1^2), \quad p_2(x^{(1)}) = \mathcal{N}(x^{(1)} \mid 2, 0.1^2), \quad p_3(x^{(1)}) = \mathcal{N}(x^{(1)} \mid 5, 0.1^2) \\
p(y \mid x^{(1)}) &= \mathcal{N}(x^{(1)} \mid x^{(1)} + 0.5, 0.1^2) \\
p_1(x^{(2)} \mid x^{(1)}) &= \mathcal{N}(x^{(2)} \mid x^{(1)} + 0.1, 0.1^2), \quad p_2(x^{(2)} \mid x^{(1)}) = \mathcal{N}(x^{(2)} \mid -2x^{(1)} + 0.1, 0.1^2), \\
p_3(x^{(2)} \mid x^{(1)}, y) &= \mathcal{N}(x^{(2)} \mid x^{(1)} + y, 0.1^2).
\end{aligned}$$

The only set of invariant feature(s) across $\mathcal{E} = \{1, 2, 3\}$ is $x^{(1)}$, and the corresponding invariant feature selector is $z^* = [1, 0]$.

In the first two environments $\mathcal{E}' = \{1, 2\}$, $x^{(1)}, x^{(2)}$ are also invariant features:

$$\begin{aligned}
p_1(y \mid x^{(1)}, x^{(2)}) &= p(y \mid x^{(1)}) \\
p_2(y \mid x^{(1)}, x^{(2)}) &= p(y \mid x^{(1)})
\end{aligned}$$

since $x^{(2)} \perp y \mid x^{(1)}$ under both $p_1(x, y)$ and $p_2(x, y)$. The corresponding posterior distributions for the two scenarios are shown in Figure S2.

Effect of estimation bias. In the above examples, we observe that the posterior does not assign equal mass to multiple invariant features, despite that a uniform prior is used. This result is an artifact of estimation bias arising from finite data, which will disappear when the true models are available.

C.3 Comparison to other methods

For the experiments in § 4.3, we include details on data simulation, method implementation, and additional results in Supplementary Sections C.3.1 to C.3.3, respectively.

C.3.1 Simulation details

We describe the process to create a random set of joint distributions $\{p_e(x, y)\}_{e=1}^E$ given p and E . The reason to differentiate between various p is to control the scale of parameter

values to prevent the sampled x, y values from exploding when p increases.

1. When $p = 10$,

- (a) $actprob \sim \text{Uniform}(\{0.6, 0.7, 0.8, 0.9\})$
- (b) For $e = 1$: (i) coefficient lower bound $lb = 1$; (ii) coefficient upper bound $ub = 2.1$, (iii) noise level lower bound $\sigma_{\min} = 0.1$; (iv) noise level upper bound $\sigma_{\max}^2 = 0.2$.
- (c) Separately for $e = 2, \dots, E$: for the intervened variable (i) mean of the absolute value of the intercept $m_e \sim \text{Uniform}([0, 1])$; (ii) coefficient lower bound $lb_e = (m_e + 0.01) * 2$; (iii) coefficient upper bound $ub_e = (m_e + 0.5) * 2$; (iv) noise level lower bound $\sigma_{e,\min} \sim \text{Uniform}([0.1, 0.2])$; (v) noise level upper bound $\sigma_{e,\max} = \sigma_{e,\min} + \text{Uniform}([0.1, 0.5])$; (vi) the probability of changing the coefficient $changeprob_e \sim \text{Uniform}([0.1, 0.3])$; and (vii) the fraction of features to be intervened on $intfrac_e \sim \text{Uniform}([0.5, 1])$

2. When $p = 450$,

- (a) $actprob \sim \text{Uniform}(\{0.1, 0.15, 0.2, 0.25\})$
- (b) For $e = 1$: same as $p = 10$ case
- (c) Separately for $e = 2, \dots, E$: for the intervened variable (i) mean of the absolute value of the intercept $m_e \sim \text{Uniform}([0, 0.4])$; (ii) coefficient lower bound $lb_e = m_e + 0.01$; (iii) coefficient upper bound $ub_e = (m_e + 0.01) * 1.5$; other hyperparameters are chosen in the same way as $p = 10$ case

We set the maximum number of the true invariant features $p_{\max}^* = 5$ when $p = 10$, and $p_{\max}^* = 10$ otherwise. For all cases of p we set the minimum number of the true invariant features $p_{\min} = 1$.

C.3.2 Method implementation details

1. EILLS: We follow the implementation at <https://github.com/wmyw96/EILLS> which accompanies the original paper by Fan et al. [2023].

2. ICP: We use the implementation at <https://github.com/juangamella/icp>.
3. Hidden-ICP: We implement a PyTorch version of the original R package available at <https://cran.r-project.org/web/packages/InvariantCausalPrediction/index.html>, which accompanies the original paper by Rothenhäusler et al. [2019].
4. VI-BIP: The prior is uniform over $p = 450$ $\{z \in \{0, 1\}^p : \|z\|_0 \leq p_{\max}\}$ where $p_{\max} = 10$ in low-dimensional case ($p = 10$), and $p_{\max} = 450$ in high dimensions ($p = 450$).

We run VI-BIP with two initialization strategies for the variational parameters and choose the one with better training-set ELBO. Consider each variational parameter ϕ_i initialized as $\log \frac{\sigma_{0i}}{1-\sigma_{0i}}$ for $i = 1, \dots, p$. The two initializations are the following: (i) uninformative initialization: we set $\sigma_{0i} = \min(p_{\max}/p \times 0.9, 0.4)$ for all i to encourage sparsity without strong prior belief; and (ii) informative initialization: based on the screening step described in the main text, we assign $\sigma_{0i} = 0.5$ for the 10 screened indices and $\sigma_{0i} = 0.1$ for the remaining ones.

As discussed in Supplementary Section B.3, when the sampled z is outside of prior support, we set the corresponding objective value in Eq. 44 to -1 . We always compute analytical gradients of KL, and stochastic gradients of the likelihood component in the ELBO.

In Algorithm 2, we use $M = 20$ gradient samples per iteration and optimize using SGD. For learning rate scheduling, we employ a cyclical learning rate strategy with a basic triangular cycle without amplitude scaling. Specifically, we set a base learning rate of 1.0, a maximum learning rate of 10, and a cycle length of 1000 iterations, with 500 steps in the increasing half. This scheduler can be implemented using the PyTorch package [Paszke, 2019]:

```
torch.optim.lr_scheduler.CyclicLR(optimizer, base_lr=0.5, max_lr=10,
step_size_up=500, mode='triangular')
```

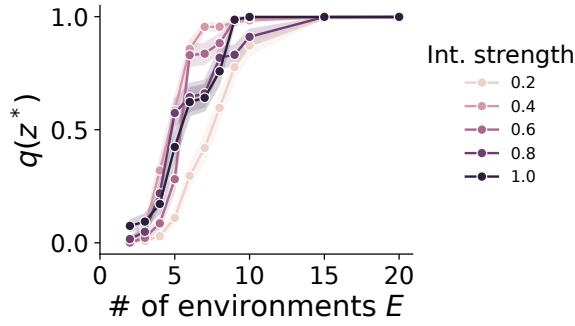


Figure S3: Synthetic study with $p = 10$ features. Variational posterior at z^* v.s. number of environments E under different fraction of intervention features. Similar to Figure 3 (B), we observe that the variational posterior also concentrates at z^* with increasing number of environments, and the convergence is faster when the fraction of intervention features is higher. The convergence of the variational posterior value at z^* is slower than that under the exact posterior shown in Figure 3 (B).

We run VI-BIP for a maximum of 2,000 iterations and select the variational parameters corresponding to the highest training-set ELBO.

C.3.3 Additional results

Figure S3 displays the variational posterior probability at the true z^* by VI-BIP for the $p = 10$ setting. Similar to the exact posterior results in Figure 3 (B), the variational posterior concentrate around z^* as the number of environments E increases, with faster convergence at under stronger interventions (which induce greater heterogeneity across environments). However, the convergence of the variational posterior probability at z^* is slower than that of the exact posterior shown in Figure 3 (B).

D Gene perturbation study

We include additional details for the experiments in § 5.

Evaluation details. We evaluate each method based on whether its predicted invariant feature gene has a significant effect on the target gene. Specifically, we say the deletion of gene j to have a significant effect on the target gene i , when (i) the deletion is successful, i.e. the expression level of gene j is above the 99% quantile or below the 1% quantile of its observational level, and (ii) the expression level of the target gene i changes significantly,

which is above the 99% quantile or below the 1% quantile of its observational level.

Hyperparameter settings in Figure 5. In Figure 5, each invariant inference method – EILLS-s, ICP-s, Hidden-ICP-s, BIP-s, and VI-BIP – is evaluated across multiple hyperparameter settings, represented by dots of varying sizes. Larger dots indicate more *conservative* settings, where the method tends to predict fewer invariant feature genes.

- EILLS-s: Higher invariance regularization parameter γ corresponds to more conservative behavior. We vary $\gamma \in [1, 25, 50, 75, 100]$.
- ICP-s: Lower significance level α results in more conservative predictions. We vary $\sigma \in [0.001, 0.005, 0.01, 0.05, 0.1]$.
- Hidden-ICP: In contrast, higher α leads to more conservative behavior. We vary $\sigma \in [0.001, 0.005, 0.01, 0.05, 0.1]$.
- BIP-s and VI-BIP: Higher posterior thresholds t lead to more conservative results. We vary $t \in [0.5, 0.6, 0.7, 0.8, 0.9]$.

Implementation details. The implementations of EILLS, ICP, and Hidden-ICP follow the same setup as described in Supplementary Section C.3.2.

For VI-BIP, we initialize the variational parameters ϕ_i to $\log \frac{\sigma_0}{1-\sigma_0}$ for $i = 1, \dots, p$, where the initial feature selection probability $\sigma_0 := 0.02$. We choose the prior to be uniform over $\{z \in \{0, 1\}^p : \|z\|_0 \leq p_{\max}\}$ with $p_{\max} = 200$. These choices are determined by coarsely searching over reasonable values guided by the optimization dynamics. A good starting point is to ensure that p_{\max} is smaller than the per-environment sample size n so that the MLEs for local conditional models are well-defined. Additionally, it is desirable that $p\sigma_0 < p_{\max}$ so that the initial expected selected features is within the prior support.

As discussed in Supplementary Section B.3, when the sampled z is outside of prior support, we set the corresponding objective value in Eq. 44 to -1 . With probability of 0.5 we compute the analytical gradients of the KL regularization term in the ELBO; otherwise we compute the stochastic gradients.

In Algorithm 2, we use $M = 10$ gradient samples per iteration and optimize using SGD. For learning rate scheduling, we employ a cyclical learning rate strategy with a basic triangular cycle that scales initial amplitude by half each cycle. Specifically, we set a base learning rate of 0.5, a maximum learning rate of 10, and a cycle length of 1000 iterations, with 500 steps in the increasing half. This scheduler can be implemented using the PyTorch package:

```
torch.optim.lr_scheduler.CyclicLR(optimizer, base_lr=0.5, max_lr=10,
    step_size_up=500, mode='triangular2')
```

We run VI-BIP for a maximum of 10,000 iterations and select the variational parameters corresponding to the highest training-set ELBO.